OPEN ACCESS

Original research

Macrophages direct cancer cells through a LOXL2-mediated metastatic cascade in pancreatic ductal adenocarcinoma

Marta Alonso-Nocelo,[1,2] Laura Ruiz-Cañas,[1,2] Patricia Sancho ,[3] Kıvanç Görgülü ,[4] Sonia Alcalá,[1,2] Coral Pedrero,[1,2] Mireia Vallespinos,[1,2] Juan Carlos López-Gil,[1,2] Marina Ochando,[1,2] Elena García-García,[5] Sara Maria David Trabulo,[6] Paola Martinelli ,[7] Patricia Sánchez-Tomero,[1,2] Carmen Sánchez-Palomo,[8] Patricia Gonzalez-Santamaría,[1,9] Lourdes Yuste,[1,2,9] Sonja Maria Wörmann,[10] Derya Kabacaoğlu,[4] Julie Earl,[11,12] Alberto Martin,[1] Fernando Salvador,[1] Sandra Valle,[1,2] Laura Martin-Hijano,[1,2] Alfredo Carrato ,[11,12,13] Mert Erkan,[14] Laura García-Bermejo,[15] Patrick C Hermann,[16] Hana Algül,[4] Gema Moreno-Bueno,[1,9,17,18] Christopher Heeschen,[6,19] Francisco Portillo,[1,17] Amparo Cano,[1,9,17] Bruno Sainz, Jr [1,2,12]

► Additional supplemental material is published online only. To view, please visit the journal online (http://dx.doi.org/10.1136/gutjnl-2021-325564).

For numbered affiliations see end of article.

Correspondence to
Dr Bruno Sainz, Jr, Departamento de Bioquímica, Universidad Autónoma de Madrid (UAM), Instituto de Investigaciones Biomédicas Alberto Sols, Madrid, Spain; bsainz@iib.uam.es

MA-N and LR-C contributed equally.

ACan and BS,J are joint senior authors.

Received 5 July 2021
Accepted 21 March 2022
Published Online First 15 April 2022

Linked

► http://dx.doi.org/10.1136/gutjnl-2022-327430

Check for updates

To cite: Alonso-Nocelo M, Ruiz-Cañas L, Sancho P, *et al*. *Gut* 2023;**72**:345–359.

ABSTRACT

Objective The lysyl oxidase-like protein 2 (LOXL2) contributes to tumour progression and metastasis in different tumour entities, but its role in pancreatic ductal adenocarcinoma (PDAC) has not been evaluated in immunocompetent in vivo PDAC models.

Design Towards this end, we used PDAC patient data sets, patient-derived xenograft in vivo and in vitro models, and four conditional genetically-engineered mouse models (GEMMS) to dissect the role of LOXL2 in PDAC. For GEMM-based studies, *K-Ras*$^{+/LSL\text{-}G12D}$;*Trp53*$^{LSL\text{-}R172H}$;*Pdx1-Cre* mice (KPC) and the *K-Ras*$^{+/LSL\text{-}G12D}$;*Pdx1-Cre* mice (KC) were crossed with *Loxl2* allele floxed mice (*Loxl2*$^{Exon2fl/fl}$) or conditional *Loxl2* overexpressing mice (R26*Loxl2*$^{KI/KI}$) to generate KPCL2^{KO} or KCL2^{KO} and KPCL2^{KI} or KCL2^{KI} mice, which were used to study overall survival; tumour incidence, burden and differentiation; metastases; epithelial to mesenchymal transition (EMT); stemness and extracellular collagen matrix (ECM) organisation.

Results Using these PDAC mouse models, we show that while *Loxl2* ablation had little effect on primary tumour development and growth, its loss significantly decreased metastasis and increased overall survival. We attribute this effect to non-cell autonomous factors, primarily ECM remodelling. *Loxl2* overexpression, on the other hand, promoted primary and metastatic tumour growth and decreased overall survival, which could be linked to increased EMT and stemness. We also identified tumour-associated macrophage-secreted oncostatin M (OSM) as an inducer of LOXL2 expression, and show that targeting macrophages in vivo affects *Osm* and *Loxl2* expression and collagen fibre alignment.

Conclusion Taken together, our findings establish novel pathophysiological roles and functions for LOXL2 in PDAC, which could be potentially exploited to treat metastatic disease.

Significance of this study

What is already known on this subject?

⇒ One of the hallmarks of the pancreatic ductal adenocarcinoma (PDAC) tumour microenvironment is an extensive desmoplastic reaction, containing a dense fibrous tissue and an abundant collagen-rich extracellular matrix (ECM), that can modulate tumour formation, progression and chemoresistance.

⇒ The lysyl oxidase family of proteins, including lysyl oxidase-like protein 2 (LOXL2), is responsible for ECM collagen and elastin crosslinking, resulting in biochemical, physical and mechanical effects that modulate tumour progression.

⇒ LOXL2 has been shown to enhance tumour progression, invasion and metastasis in a number of tumour entities via cell-autonomous mechanisms, such as activation of epithelial to mesenchymal transition (EMT), and non-cell autonomous mechanisms, such as ECM organisation.

INTRODUCTION

Pancreatic ductal adenocarcinoma (PDAC) is one of the most lethal solid tumours and one of the most frequent causes of cancer-related death worldwide.[1 2] In general, patients with PDAC have long been treated similarly, without a stratified treatment protocol, largely due to the consensus that taxonomic/molecular subtypes did not exist. This dogma, however, was challenged by numerous transcriptome studies over the past 10 years, and while the number of identified subtypes have differed across studies, two subtypes consistently appear: (1) progenitor/classical and (2) quasi-mesenchymal/squamous/basal.[3]

Although these molecular profiles have yet to impact clinical treatment decision-making, they have served to reinforce the role of the tumour

Significance of this study

What are the new findings?

⇒ Tumour-associated macrophage (TAM)-secreted oncostatin M (OSM) as an inducer of LOXL2 expression in PDAC tumours.
⇒ Loss of *Loxl2* in KRas^{G12D}-driven PDAC mouse tumours significantly decreases metastasis and increases overall survival, via non-cell autonomous factors, primarily ECM collagen remodelling.
⇒ Overexpression of *Loxl2* in KRas^{G12D}-driven PDAC mouse tumours promotes primary and metastatic tumour growth and decreases overall survival, via increased EMT and stemness.
⇒ Targeting TAMs in vivo reduces *Osm* and *Loxl2* expression, resulting in reduced metastasis.

How might it impact on clinical practice in the foreseeable future?

⇒ How and when LOXL2 is targeted in PDAC tumour development may have different implications and biological effects.
⇒ Inhibitors of LOXL2 used in combination with inhibitors of TAMs or OSM-mediated signalling may synergise in reducing the metastatic potential of PDAC tumour cells.

microenvironment (TME) in PDAC.[4–6] One of the hallmarks of PDAC is the development of a complex multicellular TME, with an extensive desmoplastic reaction, characterised by a dense fibrous tissue[7] that can exert significant biochemical, physical and mechanical effects on PDAC cells,[8] as well as an abundant extracellular matrix (ECM), composed of collagens, fibronectin, hyaluronan and tenascin C, among other components.[9] The ECM regulates tumour stiffness and organisation primarily via increased collagen deposition, crosslinking and fibre alignment. While the latter has been associated with PDAC tumour progression, chemoresistance and metastasis,[10–13] the pro-tumour role of the stroma and the ECM (ie, collagen deposition) in PDAC has been recently challenged,[14 15] highlighting our still incomplete understanding of the stroma in PDAC.

Towards this end, we set out to evaluate the role of ECM organisation in PDAC. The crosslinking of ECM collagens and elastin are primarily catalysed by the lysyl oxidase (LOX) family of proteins, composed of five members (LOX and four related enzymes, lysyl oxidase-like protein 1 (LOXL1)-4).[16–19] LOX and LOX-like proteins, specifically LOXL2, have been investigated in a number of tumour entities; however, no common universal mechanism of action has been identified for how LOX or specific LOX-like proteins enhance tumour progression, invasion and metastasis,[18–22] indicating that tumour specific as well as cell autonomous and non-cell autonomous factors are likely at play.

These challenges have impeded the translation of LOX and LOX-like protein inhibitors to the clinic, but at the same time highlight that further investigation on the role of these proteins in tumour-specific contexts are still needed. Thus, due to the pro-tumour role of collagen fibre organisation in PDAC, and our previous studies dissecting the role of LOXL2 in other tumour entities,[23–27] we took advantage of PDAC patient data sets, human patient-derived xenograft models and our previously published *Loxl2* knockout and overexpression mouse models to dissect the role of LOXL2 in PDAC tumour initiation, progression and metastasis.

METHODS

Gene expression data sets, GSEA analyses, Kaplan-Meier analysis and Pearson correlation

The gene expression data sets used in this study are publicly available. The data set from Janky *et al*[28] was downloaded from GEO (GSE62165); the data set from Moffit *et al*[4] was downloaded from GEO (GSE71729); and the META data set, containing data sets GSE15471, GSE16515, GSE22780 and GSE32688, was generated as described in ref 29.

PDAC patient-derived xenografts

Previously established PDAC patient-derived xenografts (PDAC PDX) were obtained from Dr Manuel Hidalgo under a Material Transfer Agreement with the Centro Nacional de Investigaciones Oncológicas (CNIO) (Reference no. I409181220BSMH). The indicated PDXs were expanded in female 6–8 week-old NU-Foxn1nu nude mice (Envigo, Spain) as previously described.[30] PDXs 110314, 140114 and 010414 originated from primary patient PDAC tumours resected at Rechts der Isar Hospital, Technical University of Munich and subsequently established at the CNIO.

Cell cultures

Human Panc185, Panc215, Panc253, Panc010414 and Panc354 PDAC PDX-derived cultures were established as previously described.[30] Establishment of KPC cultures has been previously described[31] and cell lines were numbered using unique identifiers (eg, ID6, ID11, ID85, ID95). KPCL2^{KO} and KPCL2^{KI} cell lines were established from explanted tumours. Briefly, tumours were minced, enzymatically digested with collagenase (Collagenase Type P, Cat no. J62406.03, Alfa Aesar) and subsequently cultured in RPMI 1640 media (Invitrogen, Cat no. 61870044) containing 10% fetal bovine serum (Invitrogen) and 50 units/mL penicillin/streptomycin (Invitrogen, Cat no. 11548876). Epithelial clones were picked, pooled, further expanded to a heterogeneous cancer cell line, re-genotyped as described[26] and numbered using unique identifiers (eg, ID11, ID32, ID86).

Genetically-engineered mouse models

The murine models of PDAC: *K-Ras*$^{+/LSL-G12D}$;*Trp53*$^{LSL-R172H}$;*Pdx1-Cre* mouse model (KPC) and the *K-Ras*$^{+/LSL-G12D}$;*Pdx1-Cre* mouse model (KC) have been described previously,[32] and were kept on a C57BL/6 background. The floxed *Loxl2* allele (exon 2) mice *Loxl2*$^{fl/fl}$ and the conditional *Loxl2-EGFP* overexpressing mouse model R26*Loxl2-EGFP*$^{KI/KI}$ have been previously described,[26] and were kept on mixed backgrounds. For advanced PDAC studies, tumour mice were generated by breeding male KPC mice with female *Loxl2*$^{Exon2fl/fl}$ to generate heterozygous (Het) KPCL2^{KO} mice (KPCL2$^{+/-}$) or with female R26*Loxl2*$^{KI/KI}$ mice to generate Het KPCL2^{KI} mice (KPCL2$^{+/KI}$). Progeny were born with expected ratios and KPCL2^{KO} mice showed no visual functional defects or abnormal pancreatic histology (data not shown). Het mice from different breedings were further crossed to obtain KPCL2$^{+/+}$, KPCL2$^{+/-}$ and KPCL2$^{-/-}$ mice for *Loxl2* depletion studies or to obtain KPCL2$^{+/+}$, KPCL2$^{+/KI}$, and KPCL2$^{KI/KI}$ mice for *Loxl2* overexpression studies. Genotyping primers used are listed in online supplemental table S2. Wild type (+/+) litter mates from both KPCL2^{KO} and KPCL2^{KI} lines were included as controls for all experiments. For tumour burden and metastasis analyses, mice were sacrificed at 17–18 weeks post birth (cohort 2). Organs, tumour and macroscopic metastases were isolated/determined, weighed and digitally documented. Tissues were fixed in 4%

paraformaldehyde, snap frozen or digested as described above to establish primary cell lines. For survival curves analyses, only mice sacrificed at humane endpoints and that developed pancreatic tumours were included (cohort 1), all others were excluded from the analyses.

A less aggressive PDAC model was also employed. For these studies male KC mice were mated with female *Loxl2*$^{Exon2fl/fl}$ to generate Het KCL2^{KO} mice (KCL2$^{+/-}$) or with female R26*Loxl2*$^{KI/KI}$ mice to generate Het KCL2^{KI} mice (KCL2$^{+/KI}$). Het mice from different breedings were further crossed to obtain KCL2$^{+/+}$, KCL2$^{+/-}$and KCL2$^{-/-}$ mice for *Loxl2* depletion studies or to obtain KCL2$^{+/+}$, KCL2$^{+/KI}$ and KCL2$^{KI/KI}$ mice for *Loxl2* overexpression studies. Wild type (+/+) litter mates from both KCL2^{KO} and KCL2^{KI} lines were included as controls for all experiments. For tumour burden and metastasis analyses, cohort 2 mice were sacrificed at 38–40 weeks post birth, and animals were processed as described above. For survival curves analyses, only mice sacrificed at humane endpoints were included (cohort 1).

Differences in the kinetics of tumour formation as well as in the percentage of mice exhibiting metastases across the wild type KPCL2^{KO} and KPCL2^{KI} and KCL2^{KO} and KCL2^{KI} lines were observed, and determined to be due to background differences.

Patient and public involvement in research

Neither patients nor the public were directly involved in this research. Included are patient samples that were provided with informed consent via the BioBank Hospital Ramón y Cajal-IRYCIS (PT13/0010/0002), integrated in the Spanish National Biobanks Network (ISCIII Biobank Register No. B.0000678) (detailed further in supplementary methods).

Statistical analyses

Results are presented as means±SEM unless stated otherwise. Pair-wise multiple comparisons were performed with one-way analysis of variance with Tukey or Dunnett's post-tests. Unless otherwise stated, unpaired two-sided (CI of 95%) Student's t-tests were used to determine differences between the means of two groups. P values<0.05 were considered statistically significant. All analyses were performed using GraphPad Prism V.6.0.

Additional methods can be found in online supplemental material.

RESULTS

LOXL2 messenger RNA expression correlates with poor overall survival and epithelial to mesenchymal transition in patients with PDAC

The transcriptional levels of *LOXL2* expression were first evaluated in three publicly available transcriptome data sets GSE62165,[28] META data set[29] and GSE71729,[4] and in line with previous publications,[33–35] *LOXL2* expression was significantly elevated in whole pancreatic tumour samples versus adjacent normal tissue (figure 1A). This increase was independently validated at the messenger RNA (mRNA) and protein levels in a previously published series[31] of freshly resected PDAC tumours (figure 1B and online supplemental figure S1A,B). Regarding survival, a clear deviation and decrease in median overall survival (OS) was observed for *LOXL2*-high expressing patients (50-percentile) compared with the *LOXL2*-low expressing patients (50-percentile) in the Bailey *et al* series[36] (figure 1C). Moreover, *LOXL2* expression was higher in the more aggressive squamous subtype versus the other three subtypes (figure 1D), as classified by Bailey *et al*.[36] Gene Set Enrichment Analysis (GSEA) comparing the samples belonging to the top and bottom quartiles of *LOXL2* expression for the three aforementioned data sets was performed, and we observed significantly and commonly enriched pathways across all series (online supplemental figure S2A), with epithelial to mesenchymal transition (EMT) and transforming growth factor-beta (TGFß) signalling being consistently and significantly enriched across all *LOXL2* high expressing patients, independent of the data set analysed (figure 1E and online supplemental figure S2A,B). Regarding EMT, a Spearman's rank-order correlation or Pearson correlation matrix of epithelial and mesenchymal genes in patients sorted for *LOXL2* mRNA levels and subjected to supervised hierarchical clustering (Euclidean distance measurement, average linkage clustering) confirmed a positive correlation in *LOXL2* mRNA expression levels with EMT and mesenchymal genes, respectively (online supplemental figure S3A and figure 1F). Likewise, high levels of *LOXL2* correlated with significantly worse survival and interval parameters (online supplemental figure S3B).

Macrophages induce LOXL2 and EMT in PDX-derived PDAC cells via OSM

Next, we analysed the levels of LOXL2 protein in a panel of PDAC PDX tumours as a model system. Of the 11 PDX tumours analysed, only the highly metastatic 265 PDX model[37] expressed LOXL2 (figure 2A), suggesting that xenografts either lose LOXL2 during in vivo passaging, a human specific TME factor that mediates LOXL2 expression is lacking in mice and/or a TME factor is lacking in culture. Building on our previously published work showing that only human M2 macrophages (MØ) can promote EMT in human PDX-derived cells,[31] we measured LOXL2 expression in PDX-cultures incubated with MØ conditioned media (MCM) and observed a clear mesenchymal morphological transition (figure 2B) as well as increased cell scattering and motility (online supplemental videos 1 and 2), in vitro invasion (figure 2C) and in vivo liver and lung colonisation (online supplemental figure S4A,B). Transcriptionally, MCM increased the expression of several EMT transcription factors as well as proto-typical LOX, and other LOX-like transcripts, with EMT-associated LOXL2 showing the strongest upregulation (figure 2D), which was confirmed at the protein level (figure 2E).

We previously showed that MCM contains the known EMT inducer TGFß1,[31] and TGFß signalling was consistently upregulated in patients with high LOXL2 expression (ie, top quartile) (online supplemental figure S2B); however, recombinant TGFß1 (rTGFß1) treatment does not induce an EMT state or *LOXL2* expression in human PDX-derived cells (online supplemental figure S4C). Thus, we hypothesised that other MCM EMT inducing factors are likely mediating LOXL2 expression. Oncostatin M (OSM) represented a plausible alternative as (1) Junk *et al* showed that OSM is a more potent EMT inducer than TGFß1, although both converge into a similar pSTAT3/SMAD3-mediated EMT pathway,[38] (2) OSM is present in MCM (figure 2F), (3) rTGFß1 can induce MØs to secrete OSM (figure 2G), and (4) OSM is present at significantly higher levels in serum from patients with PDAC compared with healthy controls (figure 2H). Indeed, treatment of PDX-derived cells with recombinant OSM (rOSM) induced a mesenchymal morphological transition (online supplemental figure S4D) as well as increased migration (online supplemental figure S4E) and induction of EMT-related gene transcription, including LOXL2 (online supplemental figure S4C, bottom),

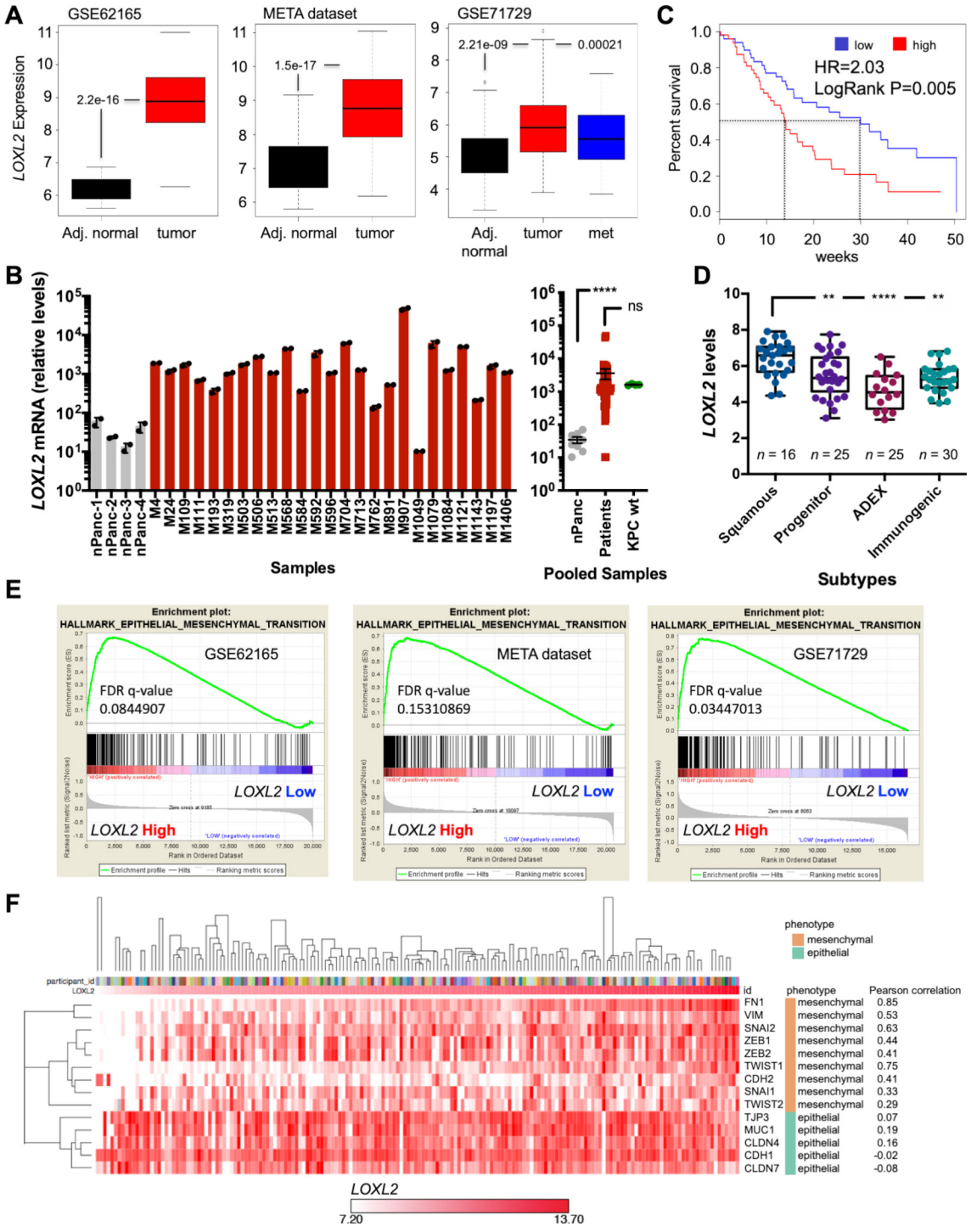

Figure 1 *LOXL2* mRNA expression correlates with poor overall survival and EMT in patients with PDAC. (A) Differential expression of *LOXL2* in adjacent (Adj.) normal tissue vs PDAC tumours and metastasis (met) in GSE62165, META data set, and GSE71729. Unpaired two-sided Student's t-test. (B) *LOXL2* relative mRNA levels ±SD (n=2 technical replicates) in a panel of surgically resected human PDAC tumours (n=25) and four normal pancreas (nPanc) controls (left). Pooled mean ±SEM analysis including four primary KPC tumours (right). (ns, not significant; ****p<0.0001; two-sided t-test with Mann-Whitney U test). (C) Overall survival of patients with PDAC from the Bailey (n=96) data set, stratified according to the median value of *LOXL2* expression. HR=Hazard ratio, Cox proportional hazard regression model. A Log-rank test was performed for survival analysis. (D) Differential expression of *LOXL2* in PDAC tumours, subtyped as progenitor, squamous, immunogenic or ADEX from the Bailey *et al* data set. (**P<0.01, ****p<0.0001, one-way analysis of variance with Dunnett post-test). (E) EMT pathway enrichment plots from transcriptomics analysis (GSE62165, META and GSE1729 data sets) of *LOXL2* high vs *LOXL2* low patients. FDR <0.25. (F) Pearson correlation matrix of mesenchymal-related and epithelial-related genes in 179 patients with human PDAC (TCGA) sorted for *LOXL2* mRNA levels and nearest neighbour. The matrix was subjected to supervised hierarchical clustering (Euclidean distance measurement, average linkage clustering). EMT, epithelial to mesenchymal transition; FDR, false discovery rate; LOXL2, lysyl oxidase-like protein 2; mRNA, messenger RNA; PDAC, pancreatic ductal adenocarcinoma; TCGA, The Cancer Genome Atlas.

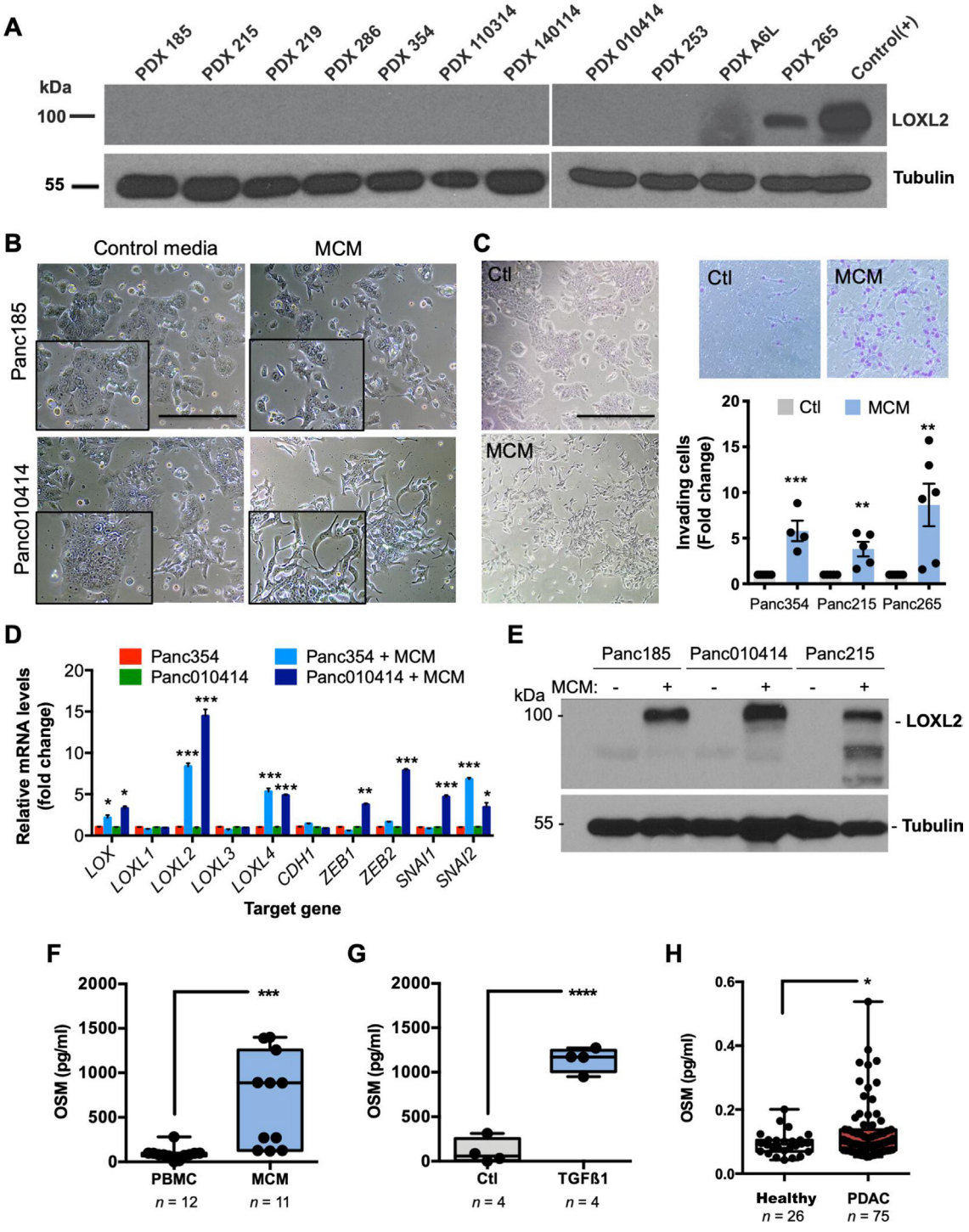

Figure 2 Macrophages induce LOXL2 and EMT in PDX-derived PDAC cells via OSM. (A) LOXL2 expression in indicated human PDXs. Tubulin, loading control. Positive (+) control=cell lysate from LOXL2-overexpressing 293T cells. (B) Light micrographs of PDX-derived cells cultured for 72 hours with control media or conditioned medium from M2-polarised MØs (MCM). Scale bar=200 µm. Insets=2X magnified areas. (C) Light micrographs of Panc354 PDX-derived cells cultured for 72 hours with control media (Ctl) or MCM (left). Scale bar=400 µm. Representative images of migrating Ctl-treated or MCM-treated cells through a 0.8 micron transwell (top, right), and mean fold-change ±SD of MCM-treated invading cells compared with Ctl-treated Panc354, Panc215 or Panc265 cells, set as 1.0. (**P<0.01, ***p<0.001, unpaired Student's t-test). (D) Mean fold-change ±SD of relative mRNA levels for the indicated genes in Ctl-treated or MCM-treated cells. Values normalised to ß-actin. Ctl-treated samples were set as 1.0. (*P<0.05, **p<0.01, ***p<0.001, unpaired Student's t-test). (E) LOXL2 expression in Ctl-treated (–) or MCM-treated (+) PDX-derived cells. Tubulin, loading control. (F–H) OSM protein levels (pg/mL) present in (F) unpolarised PBMC-conditioned media or MCM, (G) unpolarised (Ctl) PBMC-conditioned media or conditioned media from TGFß1-treated PBMCs, or (H) serum from healthy controls or patients with PDAC. (*P<0.05, ***p<0.001, ****p<0.0001, unpaired two-sided Student's t-test). EMT, epithelial to mesenchymal transition; LOXL2, lysyl oxidase-like protein 2; mRNA, messenger RNA; OSM, oncostatin M; PBMC, peripheral blood mononuclear cell; PDAC, pancreatic ductal adenocarcinoma; PDX, patient-derived xenografts; TGF, transforming growth factor.

indicating that MØ-secreted OSM can induce LOXL2 expression. We also observed a clear correlation between high OSM concentrations in MCM and pSTAT3 activation and LOXL2 protein expression (online supplemental figure S4F). Importantly, silencing of LOXL2 in Panc354 cells did not revert the capacity of rOSM or MCM to induce an EMT-like phenotype in vitro (online supplemental figure S5A-C), indicating that LOXL2 is not the downstream driver of the EMT-related phenotypes induced by both stimuli.

Loss of *Loxl2* improves OS and decreases tumour burden

Since human PDX models do not recapitulate the human TME (figure 2A), we further extrapolated our findings to a murine system. We first confirmed that four primary murine PDAC KPC (*Pdx1-cre;Kras*$^{LSL.G12D/+}$*;Tp53*$^{LSL.R172H/+}$) derived cell lines express undetectable Loxl2 levels, and that similar to human PDAC tumours and cells, murine MØ-secreted factors can induce *Loxl2* expression (online supplemental figure S6A,B). Specifically, MCM or rTGFß1 and rOSM induced Loxl2 and/or an EMT-like state in KPC cells (online supplemental figure S6B–F); however, we consistently observed that rTGFß1 was a more potent EMT inducer than rOSM in the mouse setting. Next, we crossed floxed *Loxl2* allele mice[26] with KPC mice to generate KPC; *Loxl2*$^{fl/fl}$ knockout (KO) mice (termed KPCL2^{KO}) to study the role of LOXL2 in vivo (figure 3A). Loss of *Loxl2* expression in KPCL2^{KO} tumour-derived cells or fresh tumours was confirmed by quantitative reverse transcription PCR (RT-qPCR) and western blot (WB) analysis, respectively (figure 3B,C). The levels of other Lox-like mRNAs were not affected by the loss of *Loxl2*, except for *Loxl3* (figure 3B). We next assessed OS, tumour incidence and tumour burden for KPC wild type (wt), Het *Loxl2* (KPC; *Loxl2*$^{+/-}$) and KPCL2^{KO} mice, in two different cohorts (see Methods). In the first cohort, loss of *Loxl2* significantly extended OS (figure 3D), which we conclude, from the second cohort, was not due to differences in tumour incidence (figure 3E) but rather to decreased tumour burden (figure 3F–G and online supplemental figure S7). Interestingly, *Loxl2* deletion also strongly influenced tumour differentiation. Whereas KPC tumours were heterogenous, with 64% of analysed tumours representing a more differentiated phenotype and 36% of tumours displaying a poorly differentiated phenotype, the percentage of poorly differentiated tumours was reduced to approximately 9% in KPCL2^{KO} mice (figure 3H).

Loxl2 overexpression worsens OS and increases tumour burden

We next crossed KPC mice with a previously described conditional mouse overexpressing *Loxl2*[26] to generate KPC; R26*Loxl2-EGFP*$^{KI/KI}$ knock-in (KI) mice (termed KPCL2^{KI}) (figure 4A). EGFP and Loxl2 overexpression in tumours (or cells) derived from KPC; R26$^{+/+}$, KPC; R26L2$^{+/KI}$ and KPC; R26L2$^{KI/KI}$ mice was confirmed by fluorescence microscopy, WB and RT-qPCR analysis (figure 4B,C), and overexpression of *Loxl2* did not affect the levels of other Lox-like members (figure 4C). OS, tumour incidence, and tumour burden were assessed, again using a two-cohort approach, and in contrast to KPCL2^{KO} mice, we observed decreased OS (figure 4D), increased tumour incidence (figure 4E) and significantly more tumour burden (figure 4F–H and online supplemental figure S7) when *Loxl2* was overexpressed. This increase in tumour burden coincided with a more poorly differentiated phenotype in KPC; R26L2$^{+/KI}$ and KPC; R26L2$^{KI/KI}$ mice, with 90% of KPC; R26L2$^{KI/KI}$ mice developing poorly differentiated tumours (figure 4I).

Loxl2 plays a role in initial PDAC development

Since mutant p53 accelerates tumour progression and malignant transformation via genomic instability leading to increased mutations,[39 40] we analysed the effect of *Loxl2* loss or overexpression in wt p53 KC (*Kras*$^{LSL.G12D/+}$*; Pdx1-cre*) mice that develop acinar-ductal metaplasia (ADM), pancreatic intraepithelial neoplasias (PanIN) precursor lesions, and PDAC, but at a much slower rate than KPC mice, allowing for the assessment of initial transformative events. Similar to KPC mice, loss of *Loxl2* increased OS while overexpression of *Loxl2* had the opposite effect (online supplemental figure S8A,B). Regarding pancreatic weight, only a significant increase was observed in KC; R26L2$^{KI/KI}$ mice (online supplemental figure S8C); however, at the histological level, the pancreata of 38–40 week-old KCL2^{KO} mice were predominantly composed of healthy tissue or tissue with PanIN lesions and ADM, compared with wt mice, which showed a greater and significant ($p<0.001$) percentage of PDAC lesions (online supplemental figure S8D upper, E). In KCL2^{KI} mice, a significant increase in the percentage of PDAC was observed compared with wt mice (online supplemental figure S8D bottom, F).

Loxl2 loss and overexpression affects PDAC metastasis and cancer stem cells properties

In addition to differences in tumour burden and size (figures 3 and 4), we also observed prominent differences in macroscopic metastases when *Loxl2* was modulated (figure 5A). Metastasis incidence (macroscopically and histologically confirmed, online supplemental figure S9A,B) for KPCL2^{KO} and KPCL2^{KI} mice was compared with their respective wt littermates, as the two wt KPC strains had dissimilar backgrounds that showed differences in basal metastasis. In line with survival, KPCL2^{KO} mice showed decreased liver, lung and peritoneal (intestine, lymph nodes, stomach and/or diaphragm) metastases compared with wt littermates (figure 5B). An inverse situation was observed in KPCL2^{KI} mice, with a significantly higher metastasis incidence (figure 5C), including intraperitoneal metastases, such as mesenteric lymph nodes and diaphragm metastases (figure 5A,C and online supplemental S9A,B). In the absence of mutant p53, KCL2^{KO} mice also had significantly reduced metastasis incidence, likely a direct consequence of the reduced incidence of PDAC lesions in these mice, while in KC; R26L2$^{+/KI}$ and KC; R26L2$^{KI/KI}$ mice, an increased incidence in metastasis to the liver and lung was observed (online supplemental figure S9C,D).

Expression of EMT-associated proteins have been strongly linked with PDAC metastasis.[41 42] Likewise, we have previously demonstrated an association between *Loxl2* and the EMT regulatory transcription factor *Snail1* in a breast cancer mouse model.[23] Except for an increase in the percentage of Twist1-positive cells, no difference was observed in the expression of other EMT-associated proteins analysed in KPCL2^{KO} tumours (figure 5D and online supplemental figure S10A). In the KPCL2^{KI} mice, however, expression of all proteins was increased (figure 5E and online supplemental figure S10B), in line with an increased EMT programme when *Loxl2* is overexpressed. Likewise, and as expected, a reduction in E-cadherin membrane expression was detected in tumour cells from the KPCL2^{KI} mice concordant with the more poorly differentiated morphology of these tumours (online supplemental figure S11A,B). Interestingly, when tumour-derived cultures of all four genotypes were treated with the EMT inducers TGFß1 or Osm, all cells responded to both rTGFß1- or rOSM-stimulation (although differentially) at the morphological, transcriptional and protein levels (online supplemental figure S12 and 13), indicating that

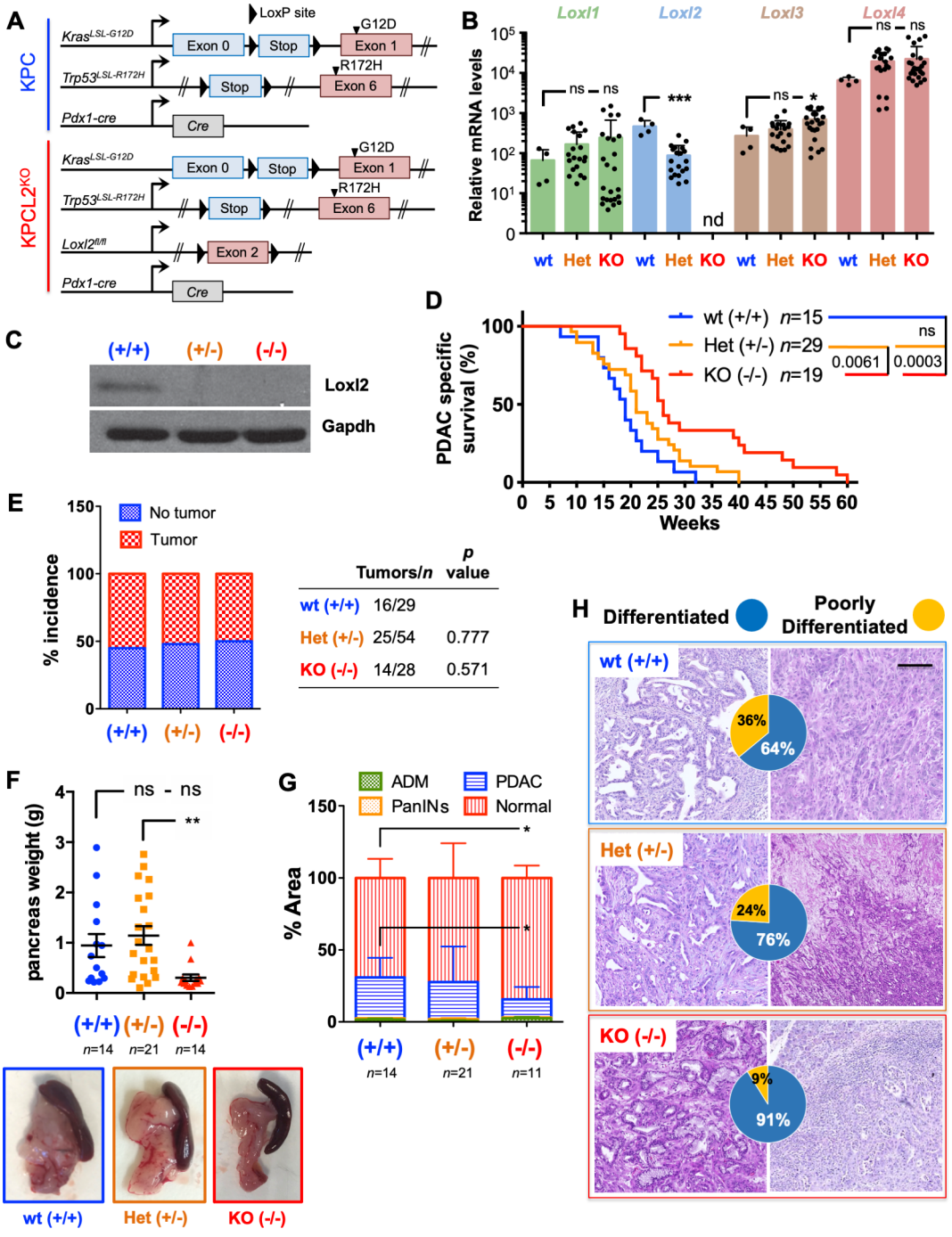

Figure 3 Loss of *Loxl2* improves overall survival and decreases tumour burden. (A) Scheme of the genetic mouse models for pancreatic cancer. The colour code (blue, KPC wild type (wt); red, KPCL2^{KO}) is used for all results. (B) Mean relative mRNA levels±SEM of indicated genes in tumour-derived cells from the indicated genotypes (nd, not detected; ns, not significant; *p<0.05, ***p<0.001; one-way analysis of variance (ANOVA) with Dunnett's post-test). (C) Loxl2 expression in tumour homogenates from the indicated KPC genotypes. Gapdh, loading control. (D) Survival of wt (+/+), Het (KPC; *Loxl2*$^{+/-}$) and KO KPC (KPC; *Loxl2*$^{-/-}$) mice. All mice died of PDAC associated disease at the indicated times (p value is shown; ns, not significant; log-rank (Mantel-Cox) test). Calculated median survivals are: wt (+/+): 19 weeks; Het (KPC; *Loxl2*$^{+/-}$): 21 weeks; and KO KPC (KPC; *Loxl2*$^{-/-}$): 26 weeks. (E) Percent tumour incidence in wt (+/+), Het (KPC; *Loxl2*$^{+/-}$) and KO KPC (KPC; *Loxl2*$^{-/-}$) mice at 17–18 weeks post birth. (P values are shown, contingency analysis, two-sided Fisher's exact test). Tumour incidence was determined as positive if a macroscopic tumour was visible on necropsy. (F) Mean pancreas weight ±SEM in wt (+/+), Het (KPC; *Loxl2*$^{+/-}$) and KO KPC (KPC; *Loxl2*$^{-/-}$) mice at 17–18 weeks post birth (left). (**P<0.01; ns, not significant; one-way ANOVA with Tukey post-test). Representative images of PDAC tumours/genotype (bottom) at 17–18 weeks post birth. (G) Quantification of tissue area in mouse pancreata from wt (+/+), Het (KPC; *Loxl2*$^{+/-}$) and KO KPC (KPC; *Loxl2*$^{-/-}$) mice at 17–18 weeks post birth, categorised as severely altered tissue (acinar-to-ductal metaplasia (ADM) and inflammation), pancreatic intraepithelial neoplasias (PanINs I–III), cancer tissue (PDAC) or normal acinar tissue (*p<0.05, contingency analysis, two-sided Fisher's exact test). (H) Representative H&E-stained sections for the grading of the respective tumours: wt (+/+) KPC (blue, n=14), Het KPC (KPC; *Loxl2*$^{+/-}$) (orange, n=21) and KO KPC (KPC; *Loxl2*$^{-/-}$) mice (red, n=11). Pie chart insets=percent of differentiated (blue) vs poorly differentiated (yellow) tumours for each genotype. Scale bar=250 µm. Het, heterozygous; KO, knockout; *Loxl2*, lysyl oxidase-like protein 2; mRNA, messenger RNA; PDAC, pancreatic ductal adenocarcinoma.

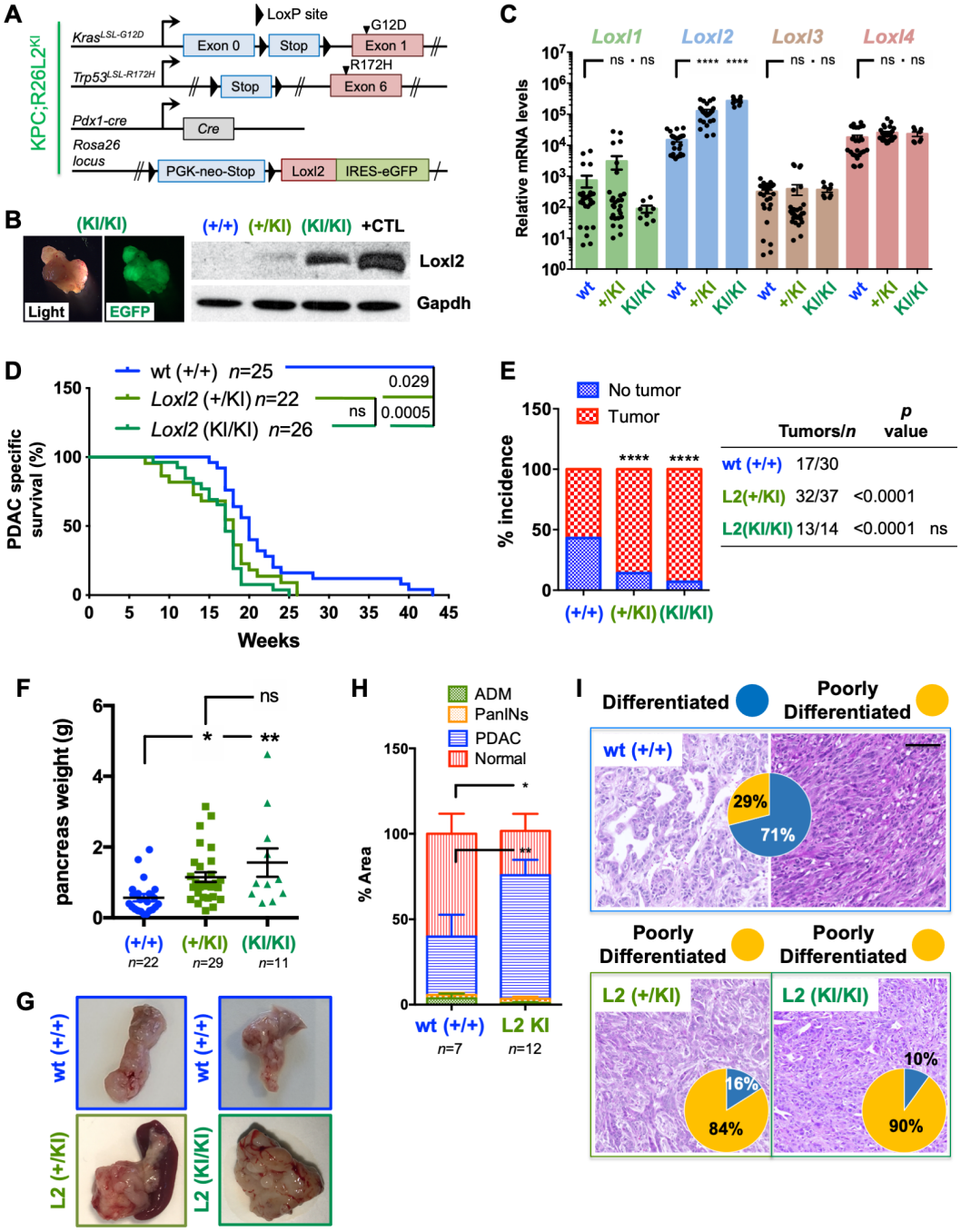

Figure 4 Overexpression of *Loxl2* worsens overall survival and increases tumour burden. (A) Scheme of the KPC-based *Loxl2* overexpression genetic mouse model. The colour code green, KPCL2^{KI}, is used for all results. (B) Light and EGFP tumour images (left). Loxl2 expression in tumour homogenates from the indicated KPC genotypes (right). Gapdh, loading control. Positive (+) control=cell lysate from murine Loxl2-overexpressing 293T cells. (C) Mean relative mRNA levels ±SEM of indicated genes in tumour-derived cells from the indicated genotypes (***p<0.001; ns, not significant; one-way analysis of variance (ANOVA) with Dunnett's post-test). (D) Survival of KPC wild type (+/+), KPC; R26L2$^{+/KI}$ and KPC; R26L2$^{KI/KI}$ mice. All mice died of PDAC associated disease at the indicated times (p value is shown; ns, not significant; log-rank (Mantel-Cox) test). Calculated median survivals are: wild type (+/+): 20 weeks; KPC; R26L2$^{+/KI}$: 18 weeks; and KPC; R26L2$^{KI/KI}$: 17 weeks. (E) Percent tumour incidence in KPC wild type (+/+), KPC; R26L2$^{+/KI}$ and KPC; R26L2$^{KI/KI}$ mice at 17–18 weeks post birth. (****P<0.0001; ns, not significant; contingency analysis; two-sided Fisher's exact test). Tumour incidence was determined as positive if a macroscopic tumour was visible on necropsy. (F) Mean pancreas weight ±SEM in KPC wild type (+/+), KPC; R26L2$^{+/KI}$ and KPC; R26L2$^{KI/KI}$ mice at 17–18 weeks post birth. (*P<0.05, **p<0.01; ns, not significant; one-way ANOVA with Tukey post-test). (G) Representative images of PDAC tumours/genotype at 17–18 weeks post birth. (H) Quantification of tissue area in mouse pancreata from wild type (+/+) KPC mice (blue, n=7) and KPCL2^{KI} (KPC; R26L2$^{+/KI}$ and KPC; R26L2$^{KI/KI}$) mice (green, n=12) determined at 17–18 weeks post birth, categorised as severely altered tissue, PanINs I–III, PDAC or normal acinar tissue (*p<0.05, **p<0.01, contingency analysis, two-sided Fisher's exact test). (I) Representative H&E-stained sections for the grading of the respective tumours: wild type (+/+) KPC (blue, n=6), KPC; R26L2$^{+/KI}$ (dark green, n=6) and KPC; R26L2$^{KI/KI}$ mice (light green, n=6). Pie chart insets=percent of differentiated (blue) vs poorly differentiated (yellow) tumours the indicated genotypes. Scale bar=250 µm. ADM, acinar-to-ductal metaplasia; KI,knock-in; *Loxl2*, lysyl oxidase-like protein 2; PanINS, pancreatic intraepithelial neoplasias; PDAC, pancreatic ductal adenocarcinoma; wt, wild type.

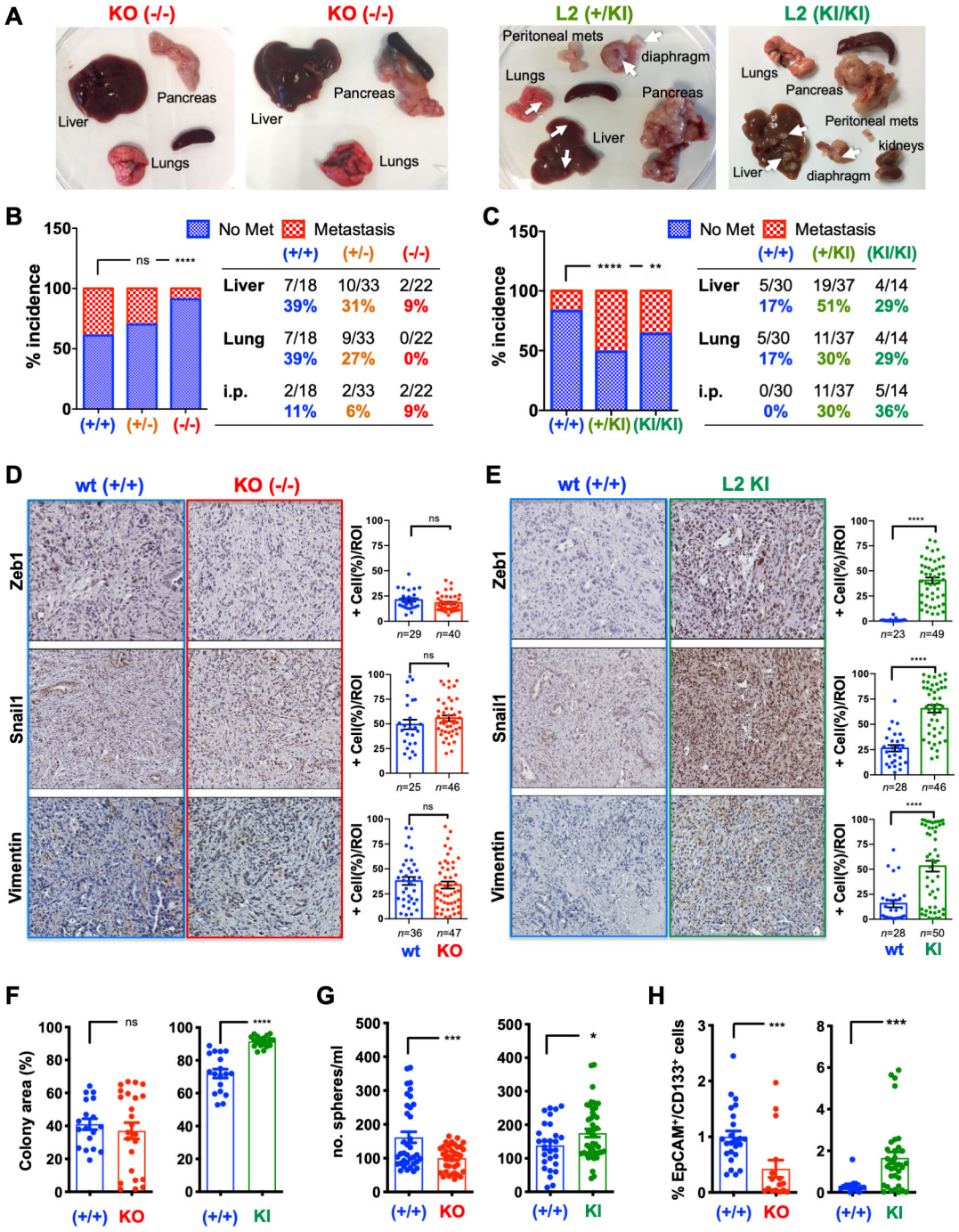

Figure 5 *Loxl2* loss and overexpression affects PDAC metastasis and cancer stem cells properties. (A) PDAC tumours and metastases from indicated genotypes (white arrows, metastases). (B–C) Percent incidence of metastasis in (B) wild type (+/+), Het (KPC; *Loxl2*$^{+/-}$) and KO KPC (KPC; *Loxl2*$^{-/-}$) mice or (C) KPC wild type (+/+), KPC; R26L2$^{+/KI}$ and KPC; R26L2$^{KI/KI}$ mice at 17–18 weeks post birth. (**P<0.01, ****p<0.0001; ns, not significant; contingency analysis, two-sided Fisher's exact test). (D–E) Left: Representative immunohistochemical stainings for indicated proteins in tumour sections from (D) wild type (+/+) KPC and KO KPC (KPC; *Loxl2*$^{-/-}$) mice or (E) wild type (+/+) KPC and KPCL2^{KI} (KPC; R26L2$^{KI/KI}$) mice. Scale bar=250 µm. Right: Quantification of per cent positive (+) cells/region of interest (ROI). (****P<0.0001; ns, not significant; unpaired Student's t-test). (F) Mean number % colony area ±SEM, determined 11 days post seeding in indicated cell lines (n=3 cell lines/genotype, ****p<0.0001, ns, not significant, two-sided t-test with Mann-Whitney U test). (G) Mean number (no.) spheres/mL ±SEM, 7 days post seeding, in tumour cell lines from indicated genotypes (*p<0.05, ***p<0.001, unpaired Student's t-test). (H) Mean percentage of EpCAM+/CD133+ cells ±SEM, in tumour cell lines from indicated genotypes (***p<0.001, two-sided t-test with Mann-Whitney U test). Het, heterozygous; KI, knock-in; KO, knockout; *Loxl2*, lysyl oxidase-like protein 2; PDAC, pancreatic ductal adenocarcinoma; wt, wild type.

regardless of the presence or absence of *Loxl2*, these cells are TGFß1-responsive and Osm-responsive and EMT-competent.

We also evaluated the percentage of cancer stem cells (CSCs), known to affect tumour burden and metastasis[41] in KPCL2^{KO} and KPCL2^{KI} cultures. *Loxl2* overexpression significantly increased colony formation capacity (figure 5F), which may explain the increased weight and size of tumours observed in KPCL2^{KI} mice. Likewise, both sphere forming capacity (ie, self-renewal) and the

percentage of CSCs (determined as EpCAM+/CD133+) significantly increased in KPCL2^{KI} cells, but decreased in KPCL2^{KO} cells (figure 5G,H), suggesting that *Loxl2* expression may be linked to a CSC state. Nonetheless, while no differences in tumour frequency in an extreme limiting dilution assay were noted for KPCL2^{KO} or KPCL2^{KI} cells when compared with their respective wt controls (online supplemental figure S14A,B), significant differences in tumour size and weight were observed for injected KPCL2^{KO} cells (online supplemental figure S14A), suggesting decreased tumour initiation and/or growth kinetics.

Loxl2 is necessary for PDAC cell intravasation

The capacity of KPCL2^{KO} and KPCL2^{KI} cells to colonise the lungs of mice on tail vein injection was measured to determine their experimental metastatic capacity. Neither the presence nor absence of *Loxl2* affected the metastatic capacity of KPCL2^{KO} and KPCL2^{KI} cells to form lung metastases in vivo (figure 6A,B), indicating that *Loxl2* expression does not influence experimental metastatic capacity (ie, extravasation, seeding and colonisation) of PDAC-derived cells injected into circulation but rather may

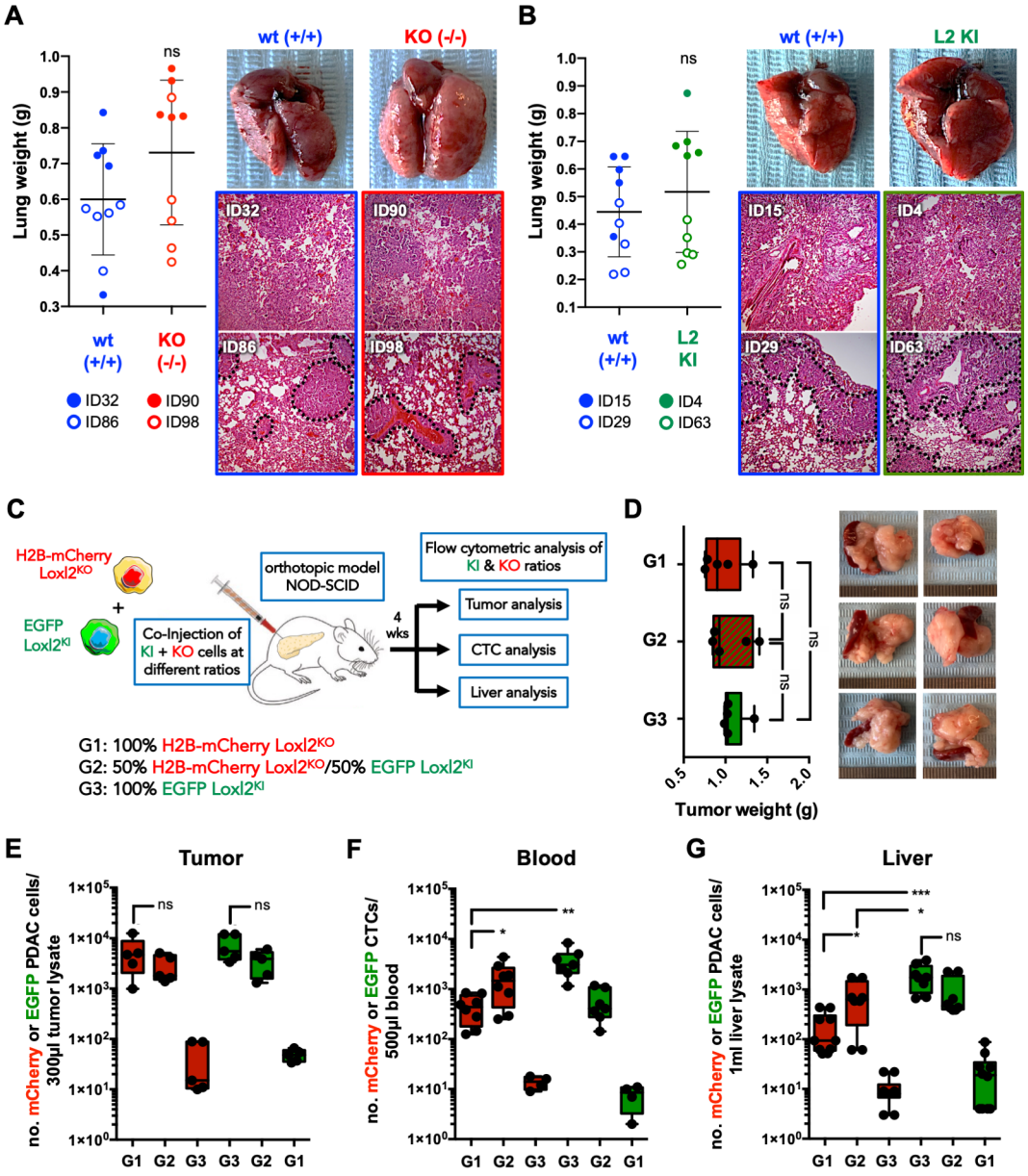

Figure 6 *Loxl2* is necessary for PDAC intravasation. (A–B) Mean lung tumour weight ±SD in (A) wild type (+/+, ID32) KPC and Het KPC (KPC; *Loxl2*$^{+/-}$, ID86) cells (blue) and KO KPC (KPC; *Loxl2*$^{-/-}$, ID90 and ID98) cells (red) or (B) wild type (+/+, ID15 and ID29) KPC cells (blue) and KPCL2^{KI} (KPC; R26L2$^{+/KI}$, ID63 and KPC; R26L2$^{KI/KI}$, ID4) cells (green) at 4 weeks post injection in NOD-SCID immunodeficient mice (left) (ns, not significant; unpaired Student's t-test). Representative images of extracted lungs (top, right) and H&E images (bottom, right). (C) Experimental set-up for in vivo orthotopic tumour establishment in NOD-SCID immunodeficient mice with H2b-mCherry-labelled KPCL2^{KO} (KPC; *Loxl2*$^{-/-}$) cells or EGFP+KPCL2^{KI} (KPC; R26L2$^{KI/KI}$) cells, alone or at a 1:1 ratio (groups 1, 3 and 2, respectively). (D) Mean tumour weight ±SD, 4 weeks post orthotopic injection, for each group (n=5 mice per group) (left). Representative images of PDAC tumours (right). (E–G) Mean number (no.) of mCherry-positive (red) or EGFP-positive (green) cells in (E) tumour homogenates, (F) blood or (G) liver homogenates, in indicated groups (*p<0.05, **p<0.01, ***p<0.001; ns, not significant; unpaired Student's t-test). Het, heterozygous; KI, knock-in; KO, knockout; *Loxl2*, lysyl oxidase-like protein 2; PDAC, pancreatic ductal adenocarcinoma; wt, wild type.

be impeding or promoting the invasion and/or intravasation of primary tumour cells through non-cell autonomous mechanisms. Therefore, we first confirmed Loxl2 secretion by KPCL2^{KI} cells and not KPCL2^{KO} cells (online supplemental figure S14C), and next established orthotopic tumours in vivo by injecting H2b-mCherry-labelled KPCL2^{KO} or EGFP+KPCL2^{KI} cells, individually or combined at a 1:1 ratio (figure 6C). If KPCL2^{KO} cells have a decreased capacity to intravasate due to a lack of extracellular Loxl2, exogenous Loxl2 expression by KPCL2^{KI} cells should rescue this phenotype. Four weeks post injection, tumours of equal weights formed in all mice (figure 6D), with the expected distribution of mCherry-positive and EGFP-positive cells (figure 6E). As hypothesised, H2b-mCherry-labelled KPCL2^{KO} cells were present at significantly lower numbers in circulation compared with EGFP+KPCL2^{KI} cells, (figure 6F); however, a significant increase in mCherry-positive cells was detected in both the blood and liver of mice when tumours were established at a 1:1 ratio with EGFP+KPCL2^{KI} cells (figure 6F,G), confirming that KPCL2^{KO} cells are able to intravasate and seed the liver when exogenous Loxl2 is provided.

Loxl2 affects collagen fibre orientation and premetastatic niche formation

The metastasis-promoting actions of LOX and LOX-like proteins in different tumour systems have been associated with extracellular functions such as ECM organisation, specifically collagen fibre crosslinking leading to tissue stiffness [reviewed in[19 43]]. Indeed, stiff tumours with high epithelial tension have been correlated with a more aggressive PDAC phenotype resulting in shorter patient survival,[10] and primary tumour ECM organisation can enhance the secretion of factors (eg, exosomes), facilitating premetastatic niche conditioning in secondary organs either through ECM remodelling or stroma cell recruitment, ultimately facilitating metastasis.

Therefore, we first analysed the myeloid-derived MØ population in livers, which has been shown to be essential in PDAC cell metastasis,[44 45] as a potential explanation for the difference observed in metastasis in KPCL2^{KO} and KPCL2^{KI} mice. Analyses revealed a negative and positive correlation between the presence of CD45^{+}CD11b^{+}F4/80^{+} cells[46] in KPCL2^{KO} and KPCL2^{KI} mice, respectively (figure 7A). We also evaluated the ECM of PDAC tumours, specifically collagen fibre directionality/organisation, which has been directly linked to Loxl2 and tumour cells.[47] While the directionality histograms for both KPCL2^{wt} and KPCL2^{KI} tumours portrayed single dominant peaks at specific/preferred orientations, KPCL2^{KO} tumours contained multiple peaks, indicating a completely isotropic behaviour (figure 7B, insets). Quantification of relative peak frequencies confirmed a significantly less organised ECM in the absence of *Loxl2* and increased organisation when overexpressed (figure 7C). In line with differential collagen fibre alignment, we observed a significant increase in pSTAT3 and pFAK in KPCL2^{KI} tumours and decreased expression of pSTAT3 and a trend towards less pFAK in KPCL2^{KO} tumours (online supplemental figure S15A,B), indicating a difference in epithelial tension and stiffness when *Loxl2* is modulated.[10 14 48] We also assessed mechanocontractility by staining for pMLC-2,[48] and observed a higher expression of active pMLC-2 in KPCL2^{KI} versus KPCL2^{KO} tumours (online supplemental figure S15A,B). Finally, to have a more general idea of the immune TME in KPCL2^{KO} and KPCL2^{KI} mice, we performed immunohistochemistry (IHC) and flow cytometry analysis (online supplemental figure S16). We did observe differences in the immune TME when comparing KPCL2^{KI} and KPCL2^{KO} tumours to their respective wt littermate controls. Interestingly, we observed increased staining for CD3 in KPCL2^{KO} and KPCL2^{KI} tumours (online supplemental figure S16A,B), which could be validated by flow cytometry (online supplemental figure S16C,D). Likewise, the macrophage population (ie, F4/80+) and specifically the M2 subpopulation (ie, CD206+) increased in the KPCL2^{KI} tumours and decreased in the KPCL2^{KO} model, compared with their respective wt litter mate controls and depending on the method used (online supplemental figure S16A–D). Lastly, while CD45 IHC staining was not robust in the formalin-fixed, paraffin-embedded (FFPE) samples, flow cytometric analysis of CD45 in KPCL2^{KO} and KPCL2^{KI} tumours showed a significant decrease and increase, respectively, compared with their respective wt controls. Thus, it appears that the lack or overexpression of *Loxl2* does affect the TME immune cell profile; however, a more exhaustive analysis would need to be performed on mice with similar genetic backgrounds before any definitive conclusions can be made.

Finally, using a syngeneic orthotopic PDAC xenograft model, mice were treated with control or clodronate liposomes to eliminate MØs (figure 7D), as we have previously reported.[49] Indeed, a significant reduction in *Osm* and *Loxl2* expression (figure 7E) was measured in PDAC tumours from clodronate-treated mice, concomitant with a significant decrease in collagen fibril orientation (figure 7F), decreased relative peak frequencies (figure 7G), and reduced overall metastasis (figure 7H), confirming that MØs produce Osm, inducing *Loxl2* expression and facilitating proper ECM organisation, which is necessary for metastasis.

DISCUSSION

Herein, we focused on LOXL2 as previously published studies have shown LOXL2 to be overexpressed and secreted in PDAC samples or cell lines,[50 51] and its expression has been positively correlated with PDAC metastasis and chemoresistance.[33 52–54] However, the majority of these studies were either observational or based on small interfering RNA silencing of LOXL2 in established PDAC cell lines. Likewise, no study to date has genetically examined the role of LOXL2 in immunocompetent mouse models of PDAC that recapitulate all aspects of the human disease.

The use of mouse models to accurately study the role of Loxl2 in PDAC is underscored by our observation that human PDAC PDXs and PDX-derived cell lines express low to undetectable LOXL2 protein levels. Similar results in established PDAC cell lines have been observed by others, with various studies concurring that only mesenchymal-like PDAC cells (eg, MiaPaCa and Panc1) express LOXL2.[33 54] Along these lines, only Panc265, a PDX recently shown to be highly metastatic in vivo,[37] expressed LOXL2. Thus, we generated immunocompetent KPC and KC mice that lacked and overexpressed *Loxl2* to accurately study *Loxl2* in an in vivo setting. The most striking consequence of Loxl2 depletion and overexpression was the inhibition and enhancement of metastasis, respectively, which translated into increased and decreased OS in KCL2^{KO}/KPCL2^{KO} and KCL2^{KI}/KPCL2^{KI} mice, respectively. We also observed clear differences in the in vivo intratumoral heterogeneity between genotypes, with KPCL2^{KI} mice giving rise to more poorly differentiated tumours with increased expression of EMT factors. The latter correlates with the observation that *LOXL2* is more highly expressed in squamous PDAC tumours, which are characterised by increased invasiveness, EMT and decreased OS. We have also previously demonstrated a relation between Loxl2/dedifferentiation in polyomavirus middle T antigen (PyMT) tumours,[23] and

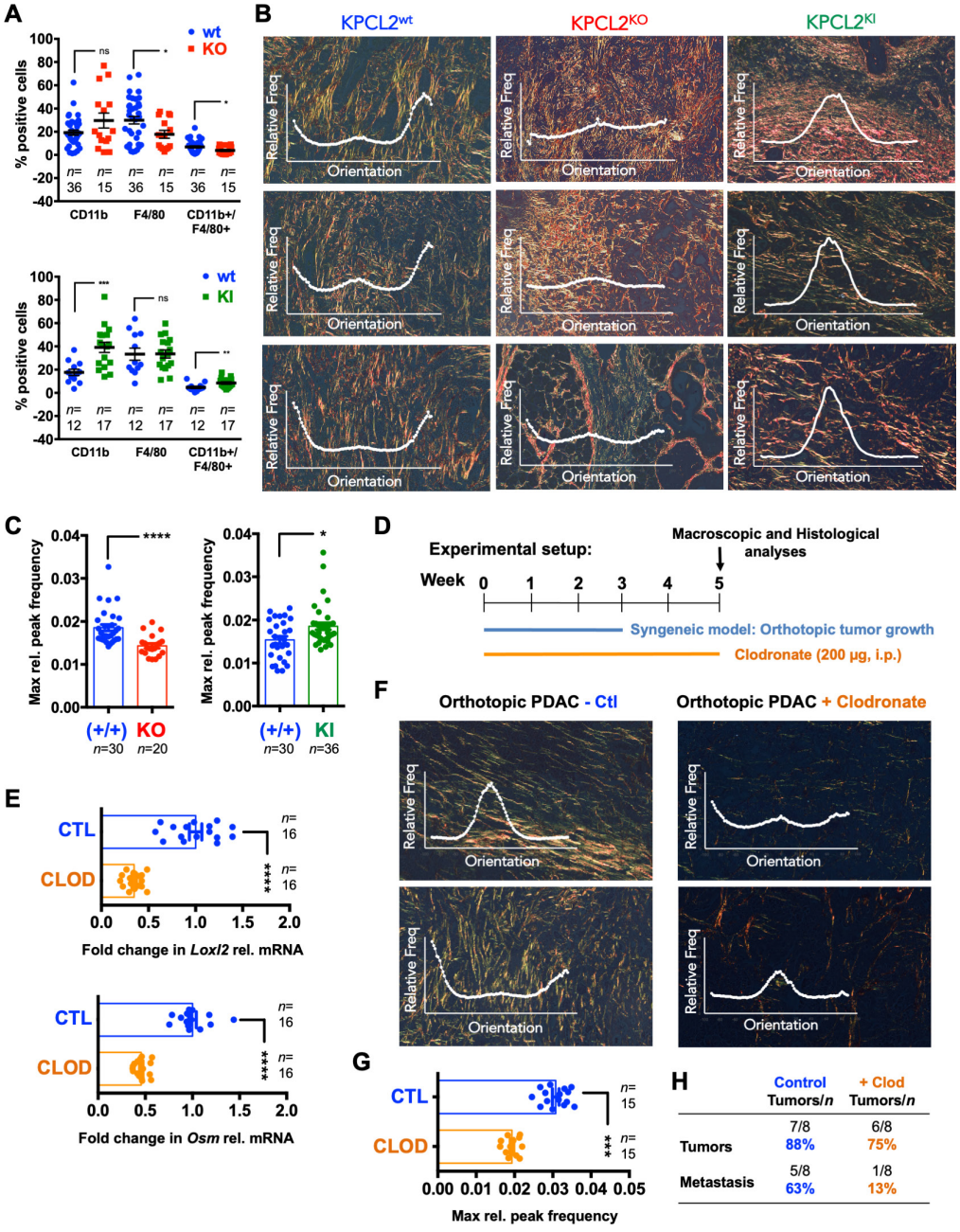

Figure 7 Loxl2 affects collagen fibre orientation and premetastatic niche formation. (A) Mean percent (%) CD11b+, F4/80+ or CD11b+/F4/80+ cells ±SEM in liver homogenates from (top) wild type (+/+) KPC and Het KPC (KPC; *Loxl2*$^{+/-}$) mice (blue) and KO KPC (KPC; *Loxl2*$^{-/-}$) mice (red) or (bottom) wild type (+/+) KPC mice (blue) and KPCL2^{KI} (KPC; R26L2$^{+/KI}$ and KPC; R26L2$^{KI/KI}$) mice (green) determined at 14–16 weeks post birth. (*P<0.05, **p<0.01, ***p<0.001; ns, not significant; two-sided t-test with Mann-Whitney U test). (B) Representative picrosirius red-stained images of pancreata. Overlay, representative fibre directionality analysis plots depicting the frequency of fibres in a specific orientation. (C) Mean maximum relative (max rel.) peak frequency ±SEM of directionality analysis plots for picrosirius red-stained images of pancreata shown in (B). (n=5–6 mice per genotype with 4–6 representative images analysed per mouse, *p<0.05, ****p<0.0001, two-sided t-test with Mann-Whitney U test). (D) Experimental set-up for clodronate (Clod) in vivo studies. (E) Mean fold-change in *Loxl2* (top) or *Osm* (bottom) relative mRNA levels ±SEM in pancreata from control liposome-treated vs clodronate liposome-treated KPC wt mice. Values were normalised to *Hprt* levels and control liposome-treated samples were set as 1.0. (n=8 mice per group, ****p<0.0001, two-sided t-test with Mann-Whitney U test). (F) Representative picrosirius red-stained images of pancreata and overlaid fibre directionality analysis plots from control (Ctl)- and clodronate-treated KPC wt mice. (G) Mean maximum relative (max rel.) peak frequency ±SEM of directionality analysis plots for picrosirius red-stained images of pancreata shown in (F). (n=5 mice per group with three representative images analysed per mouse, ***p<0.001, two-sided t-test with Mann-Whitney U test). (H) Number of tumours and metastases detected in indicated groups. Het, heterozygous; *Hprt*, hypoxanthine phosphoribosyltransferase 1; KI, knock-in; KO, knockout; *Loxl2*, lysyl oxidase-like protein 2; mRNA, messenger RNA; *Osm*, oncostatin M; PDAC, pancreatic ductal adenocarcinoma; wt, wild type.

have described positive regulatory effects of Loxl2 on EMT in general and specifically on the stability and functional activity of Snail1.[23 25] Moreover, a positive relationship was observed in KPCL2^{KI} cells at the level of stemness. Thus, increased EMT and stemness could explain the enhanced metastasis observed in KPCL2^{KI} mice.

Interestingly, KPCL2^{KO} and wt tumours expressed similar levels of EMT-associated proteins and responded similarly to the EMT inducers TGFß1 or Osm. Likewise, KPCL2^{KO} cells were able to colonise and form lung macrometastases to similar levels as wt KPC and KPCL2^{KI} cells despite their reduced 'stemness', indicating that cell-autonomous Loxl2 does not influence the EMT-responsiveness or metastatic capacity of these cells. However, since invasion and intravasation precede metastatic colonisation and growth, loss of *Loxl2* may be affecting these key early events of the metastatic cascade, which also depend on non-cell autonomous factors and processes, such as TME matrix stiffness, which can activate tumour cell EMT, invasion and metastasis.[10 55] On the other hand, and based on the data from the KCL2^{KO} mice and the ELDA tumourigenicity experiments, Loxl2 may also have an important role in tumour initiation. Nonetheless, since one of the best described functions of LOXL2 is the crosslinking, stabilisation and organisation of collagen fibres,[16] we reasoned that the reduced metastasis observed in KPCL2^{KO} mice was due primarily (but not exclusively) to extrinsic factors mediated by extracellular Loxl2. Indeed, we were able to rescue the in vivo metastatic capacity of KPCL2^{KO} tumour-derived cells by providing extracellular Loxl2 via co-injection of KPCL2^{KI} cells. Likewise, collagen fibre directionality and organisation, as well as mechanosignalling-associated proteins (pSTAT3, pFAK and pMLC-2), in KPCL2^{KO} and KPCL2^{KI} primary tumours showed opposing phenotypes, but no appreciable difference in the amount of ECM was observed, confirming that matrix organisation (and stiffness) is compromised in KPCL2^{KO} tumours. This is different to data recently reported by Collison and colleagues, where the authors show (1) that the stromal matrix restrains rather than promotes PDAC, and (2) when the ECM in a murine syngeneic PDAC model was abolished using an anti-LOXL2 mAb (AB0023, Gilead), murine PDAC progression was augmented,[14] which the authors attribute to a reduction in the ECM content and fibrosis. Recently, Kalluri and colleagues also showed that depletion of myofibroblast-derived Col1 in vivo accelerated the emergence of PanINs and PDAC.[15]

In our study, KPCL2^{KO} mice had improved OS and reduced metastasis while the reverse occurred in KPCL2^{KI} mice. It is important to note that in KPCL2^{KO} mice, *Loxl2* was genetically deleted only in PDAC cells and from birth, thus a direct comparison with the Jiang *et al* study[14] cannot be made. Likewise, we cannot rule out that other cell types present in the TME may represent alternate sources of Loxl2; however, this potential contribution was likely minimal as collagen fibre crosslinking and organisation was consistently compromised in KPCL2^{KO} tumours. In our syngeneic PDAC in vivo system, while collagen fibre misalignment and reduced *Loxl2* was achieved with clodronate treatment, similar to the study by,[14] PDAC metastasis was not augmented but rather reduced. The latter may be a consequence of the additional macrophage depletion mediated by the clodronate liposomes, which others have shown to be necessary for PDAC metastasis.[56] In fact, we observed that the immune TME was affected by *Loxl2* levels, which may have contributed to the observed in vivo phenotypes independent of, or in combination with, ECM organisation. Lastly, results from a 2017 randomised phase II study of simtuzumab, a humanised IgG4 monoclonal antibody (derived from AB0023) that inhibits extracellular LOXL2, in combination with gemcitabine for first-line treatment of patients with metastatic PDAC (ClinicalTrials.gov, NCT01472198), indicated that the addition of simtuzumab to gemcitabine did not improve clinical outcomes[57]; however, the combination approach did not accelerate tumour progression. Thus, these differing views regarding the role of LOXL2 in PDAC tumourigenesis highlight the complex interplay of tumour-stroma interactions and the need to further understand this crosstalk as well as to re-evaluate the utility of anti-LOXL2 antibodies or small molecule LOXL2 inhibitors[58] in the treatment of metastatic PDAC.

We additionally identify in this study macrophages and OSM as important players in this interplay. Interestingly, Dinca *et al* recently showed in invasive breast ductal carcinomas that OSM can induce LOXL2 expression, which in turn promotes an increase in ECM collagen I fibre crosslinking, leading to increased cell invasion.[59] Likewise, Lee *et al*, recently demonstrated that MØ-secreted Osm induces inflammatory gene expression in CAFs, creating a pro-tumourigenic environment in PDAC.[60] Interestingly, they also show that tumour cells implanted in *Osm*$^{-/-}$ mice displayed an epithelial-dominated morphology as well as reduced tumour growth and metastasis. Thus, our results not only definitively link LOXL2 expression to macrophage-secreted OSM in PDAC, but taken together, these studies highlight that targeting macrophages, OSM or both (eg, using inhibitors to target CSF1R or GP130), may provide a more effective therapeutic strategy for treating PDAC as well as circumvent potential issues associated with targeting LOXL2 alone.

Author affiliations
[1]Departament of Biochemistry, Universidad Autónoma de Madrid (UAM), Departament of Cancer Biology, Instituto de Investigaciones Biomédicas Alberto Sols CSIC-UAM, Madrid, Spain
[2]Cancer Stem Cells and Fibroinflammatory Microenvironment Group, Chronic Diseases and Cancer, Area 3, Instituto Ramón y Cajal de Investigación Sanitaria (IRYCIS), Madrid, Spain
[3]Translational Research Unit, Hospital Miguel Servet, Instituto de Investigacion Sanitaria Aragon, Zaragoza, Spain
[4]Comprehensive Cancer Center München, Klinikum rechts der Isar der Technischen Universität München, München, Germany
[5]Departamento de Anatomía Patológica, Hospital Universitario Fundación Alcorcón, Alcorcón, Spain
[6]Stem Cells and Cancer Group, Molecular Pathology Programme, Spanish National Cancer Research Centre (CNIO), Madrid, Spain
[7]Institute for Cancer Research, Comprehensive Cancer Center, Medizinische Universitat Wien, Wien, Austria
[8]Departamento de Anatomía, Histologia y Neurociencia, Universidad Autónoma de Madrid, Madrid, Spain
[9]Cancer and Human Molecular Genetics, Instituto de Investigación Sanitaria IdiPAZ, Madrid, Spain
[10]Ahmed Cancer Center for Pancreatic Cancer Research, The University of Texas MD Anderson Cancer Center, Houston, Texas, USA
[11]Molecular Epidemiology and Predictive Tumor Markers Group, Chronic Diseases and Cancer, Area 3, Instituto Ramón y Cajal de Investigación Sanitaria (IRYCIS), Madrid, Spain, Madrid, Spain
[12]Gastrointestinal Tumours Research Programme, Biomedical Research Network in Cancer (CIBERONC), Madrid, Spain
[13]Alcala University, Madrid, Spain
[14]University Research Center for Translational Medicine - KUTTAM, Istanbul, Turkey
[15]Biomarkers and Therapeutic Targets Group, Area 4, Instituto Ramón y Cajal de Investigación Sanitaria (IRYCIS), Madrid, Spain
[16]Department of Internal Medicine I, Ulm University, Ulm, Germany
[17]Breast Cancer Research Programme, Biomedical Research Network in Cancer (CIBERONC), Madrid, Spain
[18]Fundación MD Anderson Internacional, Madrid, Spain
[19]Center for Single-Cell Omics and Key Laboratory of Oncogenes and Related Genes, Shanghai Jiao Tong University School of Medicine, Shanghai, China

Twitter Kıvanç Görgülü @kivancgorgulu and Bruno Sainz, Jr @sainz_lab

Acknowledgements We thank the patients and the BioBank Hospital Ramón y Cajal-IRYCIS (PT13/0010/0002) integrated in the Spanish National Biobanks Network for its collaboration and, in particular, Adrián Povo Retana for macrophage isolation and Dr. Javier Fco. Regadera Gonzalez for histology assistance. We also thank Vanesa Bermeo, Emilio González-Arnay and Sandra Batres Ramos for their invaluable technical help with this study. SV and PS-T were recipients of fellowships from the Comunidad de Madrid, Ayudas Para La Contratación de Predoctorales y Técnicos de Laboratorio (PEJD-2017-PRE/BMD-5062 and PEJ-2017-TL/BMD-7505, respectively), Madrid, Spain.

Contributors MV initiated the study. MA-N, PS, SA, KG, MV, MO, PG-S, JCL-G, SV and LM-H performed in vitro experiments and analysed data; MV, CP, LY and LR-C performed in vivo studies and analysed data; LG-B performed RNA FFPE extractions; PM, KG and SMW performed bioinformatics analyses; KG, PS-T, CS-P and DK performed histological analyses; EGG is our in-house pathologist and assisted with in vivo histological evaluations with PCH and MO; GM-B performed IHC analyses of human PDAC tumours; CH, PS and SMDT spearheaded the OSM studies; JE and ACar performed ELISA analyses and provided primary patient serum and tumour samples; ME provided human resected tumor samples for RNA analyses; AM, FS, ACan and FP produced and characterised the Loxl2 mouse models. HA, KG, PCH and GM-B provided significant scientific input, analysed data and reviewed the manuscript. ACan, FP and BSJ developed the study concept, obtained funding, interpreted the data and drafted/edited the manuscript. BSJ acts as the guarantor, and accepts full responsibility for the finished work and/or the conduct of the study, had access to the data, and controlled the decision to publish. All authors edited the manuscript.

Funding JCL-G received support from a 'la Caixa' Foundation (ID 100010434) fellowship (LCF/BQ/DR21/11880011). This study was supported by ISCIII FIS grants PI18/00757 and PI21/01110 (BSJ) and PI18/00267 (LG-B), and grants from the Spanish Ministry of Economy and Innovation SAF2016-76504-R (ACan and FP), PID2019-111052RB-I00 (FP), PID2019-104644RB-I00 (GM-B), a Ramón y Cajal Merit Award RYC-2012–12104 (BSJ) and ISCIII, CIBERONC, CB16/12/00446 (ACar) and CB16/12/00295 (ACan and GM-B), all of them co-financed through Fondo Europeo de Desarrollo Regional (FEDER) 'Una manera de hacer Europa'; a Fero Foundation Grant (BSJ); a Coordinated grant (GC16173694BARB) from the Fundación Científica Asociación Española Contra el Cáncer (FC-AECC) (BSJ); a Miguel Servet award (CP16/00121) (PS); a DFG, German Research Foundation Grant—Project no: 492 436 553 (KG); and a Max Eder Fellowship of the German Cancer Aid (111746) (PCH)

Competing interests None declared.

Patient and public involvement Patients and/or the public were not involved in the design, or conduct, or reporting, or dissemination plans of this research.

Patient consent for publication Not applicable.

Ethics approval Expansion of human PDXs in vivo, mouse breedings and all in vivo procedures in mice were conducted in accordance with protocols approved by the local Animal Experimental Ethics Committee of the Instituto de Salud Carlos III (PA 34–2012) or the Use Committee for Animal Care from the Universidad Autónoma de Madrid (UAM) (Ref# CEI-25–587) and the Comunidad de Madrid (PROEX 335/14, 182/14 or 294/19). For all in vivo experiments, mice were housed according to institutional guidelines and all experimental procedures were performed in compliance with the institutional guidelines for the welfare of experimental animals and in accordance with the guidelines for Ethical Conduct in the Care and Use of Animals as stated in The International Guiding Principles for Biomedical Research involving Animals, developed by the Council for International Organisations of Medical Sciences (CIOMS). Blood samples from patients with PDAC and healthy donors were provided by the BioBank Hospital Ramón y Cajal-IRYCIS (PT13/0010/0002), integrated in the Spanish National Biobanks Network (ISCIII Biobank Register No. B.0000678), and by ACar from the 'Collection of samples of the Familial Pancreas Cancer Registry' of the Carlos III Institute (ISCIII ref n°:C.0003953). Samples were processed following standard operating procedures with the appropriate approval of the Ethical and Scientific Committees (Control no. No. Control: DE-BIOB-73 AC65, RG.BIOB-57 and RG.BIOB-54), with informed consent and according to Declaration of Helsinki principles. Tumours derived from surgical resections at Rechts der Isar Hospital, Technical University of Munich, were obtained with written informed consent and authorised by the Rechts der Isar Hospital Ethics Committee with Project number 1926/07 and 5510/12.

Provenance and peer review Not commissioned; externally peer reviewed.

Data availability statement Data from datasets used in this manuscript are available in a public, open access repository. Other data are available upon reasonable request. https://www.nature.com/articles/ng.3398; https://bmccancer.biomedcentral.com/articles/10.1186/s12885-016-2540-6; https://gut.bmj.com/content/66/9/1665.

ORCID iDs
Patricia Sancho http://orcid.org/0000-0002-1092-5395
Kıvanç Görgülü http://orcid.org/0000-0002-1613-1422
Paola Martinelli http://orcid.org/0000-0002-1643-8731
Alfredo Carrato http://orcid.org/0000-0001-7749-8140
Bruno Sainz, Jr http://orcid.org/0000-0003-4829-7651

REFERENCES

1 Bray F, Ferlay J, Soerjomataram I, *et al*. Global cancer statistics 2018: GLOBOCAN estimates of incidence and mortality worldwide for 36 cancers in 185 countries. *CA Cancer J Clin* 2018;68:394–424.
2 Siegel RL, Miller KD, Jemal A. Cancer statistics, 2020. *CA Cancer J Clin* 2020;70:7–30.
3 Collisson EA, Bailey P, Chang DK, *et al*. Molecular subtypes of pancreatic cancer. *Nat Rev Gastroenterol Hepatol* 2019;16:207–20.
4 Moffitt RA, Marayati R, Flate EL, *et al*. Virtual microdissection identifies distinct tumor- and stroma-specific subtypes of pancreatic ductal adenocarcinoma. *Nat Genet* 2015;47:1168–78. dataset https://www.nature.com/articles/ng.3398
5 Hosein AN, Brekken RA, Maitra A. Pancreatic cancer stroma: an update on therapeutic targeting strategies. *Nat Rev Gastroenterol Hepatol* 2020;17:487–505.
6 Puleo F, Nicolle R, Blum Y, *et al*. Stratification of pancreatic ductal adenocarcinomas based on tumor and microenvironment features. *Gastroenterology* 2018;155:1999–2013.
7 Neesse A, Algül H, Tuveson DA, *et al*. Stromal biology and therapy in pancreatic cancer: a changing paradigm. *Gut* 2015;64:1476–84.
8 Erkan M, Hausmann S, Michalski CW, *et al*. The role of stroma in pancreatic cancer: diagnostic and therapeutic implications. *Nat Rev Gastroenterol Hepatol* 2012;9:454–67.
9 Multhaupt HAB, Leitinger B, Gullberg D, *et al*. Extracellular matrix component signaling in cancer. *Adv Drug Deliv Rev* 2016;97:28–40.
10 Laklai H, Miroshnikova YA, Pickup MW, *et al*. Genotype tunes pancreatic ductal adenocarcinoma tissue tension to induce matricellular fibrosis and tumor progression. *Nat Med* 2016;22:497–505.
11 Chaudhuri PK, Low BC, Lim CT. Mechanobiology of tumor growth. *Chem Rev* 2018;118:6499–515.
12 Feig C, Gopinathan A, Neesse A, *et al*. The pancreas cancer microenvironment. *Clin Cancer Res* 2012;18:4266–76.
13 Erkan M, Michalski CW, Rieder S, *et al*. The activated stroma index is a novel and independent prognostic marker in pancreatic ductal adenocarcinoma. *Clin Gastroenterol Hepatol* 2008;6:1155–61.
14 Jiang H, Torphy RJ, Steiger K, *et al*. Pancreatic ductal adenocarcinoma progression is restrained by stromal matrix. *J Clin Invest* 2020;130:4704–9.
15 Chen Y, Kim J, Yang S, *et al*. Type I collagen deletion in αSMA^{+} myofibroblasts augments immune suppression and accelerates progression of pancreatic cancer. *Cancer Cell* 2021;39:548–65.
16 Kim Y-M, Kim E-C, Kim Y. The human lysyl oxidase-like 2 protein functions as an amine oxidase toward collagen and elastin. *Mol Biol Rep* 2011;38:145–9.
17 Lucero HA, Kagan HM. Lysyl oxidase: an oxidative enzyme and effector of cell function. *Cell Mol Life Sci* 2006;63:2304–16.
18 Moon H-J, Finney J, Ronnebaum T, *et al*. Human lysyl oxidase-like 2. *Bioorg Chem* 2014;57:231–41.
19 Cano A, Santamaría PG, Moreno-Bueno G. Loxl2 in epithelial cell plasticity and tumor progression. *Future Oncol* 2012;8:1095–108.
20 Wen B, Xu L-Y, Li E-M. LOXL2 in cancer: regulation, downstream effectors and novel roles. *Biochim Biophys Acta Rev Cancer* 2020;1874:188435.
21 Ye M, Song Y, Pan S, *et al*. Evolving roles of lysyl oxidase family in tumorigenesis and cancer therapy. *Pharmacol Ther* 2020;215:107633.
22 Lin H-Y, Li C-J, Yang Y-L, *et al*. Roles of lysyl oxidase family members in the tumor microenvironment and progression of liver cancer. *Int J Mol Sci* 2020;21. doi:10.3390/ijms21249751. [Epub ahead of print: 21 Dec 2020].
23 Salvador F, Martin A, López-Menéndez C, *et al*. Lysyl oxidase-like protein LOXL2 promotes lung metastasis of breast cancer. *Cancer Res* 2017;77:5846–59.
24 Peinado H, Moreno-Bueno G, Hardisson D, *et al*. Lysyl oxidase-like 2 as a new poor prognosis marker of squamous cell carcinomas. *Cancer Res* 2008;68:4541–50.
25 Peinado H, Del Carmen Iglesias-de la Cruz M, Olmeda D, *et al*. A molecular role for lysyl oxidase-like 2 enzyme in snail regulation and tumor progression. *Embo J* 2005;24:3446–58.
26 Martin A, Salvador F, Moreno-Bueno G, *et al*. Lysyl oxidase-like 2 represses Notch1 expression in the skin to promote squamous cell carcinoma progression. *Embo J* 2015;34:1090–109.
27 Moreno-Bueno G, Salvador F, Martín A, *et al*. Lysyl oxidase-like 2 (LOXL2), a new regulator of cell polarity required for metastatic dissemination of basal-like breast carcinomas. *EMBO Mol Med* 2011;3:528–44.
28 Janky Rekin's, Binda MM, Allemeersch J, *et al*. Prognostic relevance of molecular subtypes and master regulators in pancreatic ductal adenocarcinoma. *BMC Cancer* 2016;16:632.

29 Martinelli P, Carrillo-de Santa Pau E, Cox T, *et al*. GATA6 regulates EMT and tumour dissemination, and is a marker of response to adjuvant chemotherapy in pancreatic cancer. *Gut* 2017;66:1665–76.
30 Mueller M-T, Hermann PC, Witthauer J, *et al*. Combined targeted treatment to eliminate tumorigenic cancer stem cells in human pancreatic cancer. *Gastroenterology* 2009;137:1102–13.
31 Sainz B, Alcala S, Garcia E, *et al*. Microenvironmental hCAP-18/LL-37 promotes pancreatic ductal adenocarcinoma by activating its cancer stem cell compartment. *Gut* 2015;64:1921–35.
32 Hingorani SR, Wang L, Multani AS, *et al*. Trp53R172H and KrasG12D cooperate to promote chromosomal instability and widely metastatic pancreatic ductal adenocarcinoma in mice. *Cancer Cell* 2005;7:469–83.
33 Tanaka N, Yamada S, Sonohara F, *et al*. Clinical implications of lysyl oxidase-like protein 2 expression in pancreatic cancer. *Sci Rep* 2018;8:9846.
34 Zhang Y, Zhu L. Wang X. A network-based approach for identification of subtype-specific master regulators in pancreatic ductal adenocarcinoma. *Genes* 2020;11.
35 Kim I-K, Lee YS, Kim HS, *et al*. Specific protein 1(SP1) regulates the epithelial-mesenchymal transition via lysyl oxidase-like 2(LOXL2) in pancreatic ductal adenocarcinoma. *Sci Rep* 2019;9:5933.
36 Bailey P, Chang DK, Nones K, *et al*. Genomic analyses identify molecular subtypes of pancreatic cancer. *Nature* 2016;531:47–52.
37 Dimitrov-Markov S, Perales-Patón J, Bockorny B, *et al*. Discovery of new targets to control metastasis in pancreatic cancer by single-cell transcriptomics analysis of circulating tumor cells. *Mol Cancer Ther* 2020;19:1751–60.
38 Junk DJ, Bryson BL, Smigiel JM, *et al*. Oncostatin M promotes cancer cell plasticity through cooperative STAT3-SMAD3 signaling. *Oncogene* 2017;36:4001–13.
39 Rivlin N, Koifman G, Rotter V. P53 orchestrates between normal differentiation and cancer. *Semin Cancer Biol* 2015;32:10–17.
40 Muller PAJ, Vousden KH. Mutant p53 in cancer: new functions and therapeutic opportunities. *Cancer Cell* 2014;25:304–17.
41 Wiesmüller L, Wiesmüller L, Sainz B, *et al*. Emt and Stemness-Key players in pancreatic cancer stem cells. *Cancers* 2019;11. doi:10.3390/cancers11081136. [Epub ahead of print: 08 08 2019].
42 Krebs AM, Mitschke J, Lasierra Losada M, *et al*. The EMT-activator ZEB1 is a key factor for cell plasticity and promotes metastasis in pancreatic cancer. *Nat Cell Biol* 2017;19:518–29.
43 Chitty JL, Setargew YFI, Cox TR. Targeting the lysyl oxidases in tumour desmoplasia. *Biochem Soc Trans* 2019;47:1661–78.
44 Lee JW, Stone ML, Porrett PM, *et al*. Hepatocytes direct the formation of a pro-metastatic niche in the liver. *Nature* 2019;567:249–52.
45 Costa-Silva B, Aiello NM, Ocean AJ, *et al*. Pancreatic cancer exosomes initiate pre-metastatic niche formation in the liver. *Nat Cell Biol* 2015;17:816–26.
46 Nielsen SR, Quaranta V, Linford A, *et al*. Macrophage-Secreted granulin supports pancreatic cancer metastasis by inducing liver fibrosis. *Nat Cell Biol* 2016;18:549–60.
47 Grossman M, Ben-Chetrit N, Zhuravlev A, *et al*. Tumor cell invasion can be blocked by modulators of collagen fibril alignment that control assembly of the extracellular matrix. *Cancer Res* 2016;76:4249–58.
48 Cortes E, Lachowski D, Rice A, *et al*. Tamoxifen mechanically deactivates hepatic stellate cells via the G protein-coupled estrogen receptor. *Oncogene* 2019;38:2910–22.
49 D'Errico G, Alonso-Nocelo M, Vallespinos M, *et al*. Tumor-Associated macrophage-secreted 14-3-3ζ signals via Axl to promote pancreatic cancer chemoresistance. *Oncogene* 2019;38:5469–85.
50 Makawita S, Smith C, Batruch I, *et al*. Integrated proteomic profiling of cell line conditioned media and pancreatic juice for the identification of pancreatic cancer biomarkers. *Mol Cell Proteomics* 2011;10:M111–8599.
51 Grützmann R, Foerder M, Alldinger I, *et al*. Gene expression profiles of microdissected pancreatic ductal adenocarcinoma. *Virchows Arch* 2003;443:508–17.
52 Le Calvé B, Griveau A, Vindrieux D, *et al*. Lysyl oxidase family activity promotes resistance of pancreatic ductal adenocarcinoma to chemotherapy by limiting the intratumoral anticancer drug distribution. *Oncotarget* 2016;7:32100–12.
53 Rückert F, Joensson P, Saeger H-D, *et al*. Functional analysis of LOXL2 in pancreatic carcinoma. *Int J Colorectal Dis* 2010;25:303–11.
54 Park JS, Lee J-H, Lee YS, *et al*. Emerging role of LOXL2 in the promotion of pancreas cancer metastasis. *Oncotarget* 2016;7:42539–52.
55 Wei SC, Fattet L, Tsai JH, *et al*. Matrix stiffness drives epithelial-mesenchymal transition and tumour metastasis through a TWIST1-G3BP2 mechanotransduction pathway. *Nat Cell Biol* 2015;17:678–88.
56 Griesmann H, Drexel C, Milosevic N, *et al*. Pharmacological macrophage inhibition decreases metastasis formation in a genetic model of pancreatic cancer. *Gut* 2017;66:1278–85.
57 Benson AB, Wainberg ZA, Hecht JR, *et al*. A phase II randomized, double-blind, placebo-controlled study of Simtuzumab or placebo in combination with gemcitabine for the first-line treatment of pancreatic adenocarcinoma. *Oncologist* 2017;22:241–e15.
58 Chang J, Lucas MC, Leonte LE, *et al*. Pre-Clinical evaluation of small molecule LOXL2 inhibitors in breast cancer. *Oncotarget* 2017;8:26066–78.
59 Dinca SC, Greiner D, Weidenfeld K, *et al*. Novel mechanism for OSM-promoted extracellular matrix remodeling in breast cancer: LOXL2 upregulation and subsequent ECM alignment. *Breast Cancer Res* 2021;23:56.
60 Lee BY, Hogg EKJ, Below CR, *et al*. Heterocellular OSM-OSMR signalling reprograms fibroblasts to promote pancreatic cancer growth and metastasis. *Nat Commun* 2021;12:7336.

Macrophages direct cancer cells through a LOXL2-mediated metastatic cascade in pancreatic ductal adenocarcinoma

Marta Alonso-Nocelo, Laura Ruiz-Cañas, Patricia Sancho, Kıvanç Görgülü, Sonia Alcalá, Coral Perdero, Mireia Vallespinos, Juan Carlos López-Gil, Marina Ochando, Elena García-García, Sara Trabulo, Paola Martinelli, Patricia Sánchez-Tomero, Carmen Sánchez Palomo, Patricia G. Santamaría, Lourdes Yuste, Sonja M. Wörmann, Derya Kabacaoğlu, Julie Earl, Alberto Martin, Fernando Salvador, Sandra Valle, Laura Martin-Hijano, Alfredo Carrato, Mert Erkan, Laura Garcia-Bermejo, Patrick C. Hermann, Hana Algül, Gema Moreno-Bueno, Christopher Heeschen, Francisco Portillo, Amparo Cano, and Bruno Sainz, Jr.

SUPPLEMENTARY MATERIAL

- SUPPLEMENTARY METHODS
- SUPPLEMENTARY TABLES
- SUPPLEMENTARY REFERENCES
- SUPPLEMENTARY FIGURES AND LEGENDS
- SUPPLEMENTARY VIDEOS

SUPPLEMENTARY METHODS

Gene expression datasets, GSEA analyses, Kaplan–Meier analysis and Pearson Correlation

LOXL2 expression levels in indicated datasets were compared in adjacent normal tissue, PDAC tumor tissue and metastatic tissue (if available), and Box Whisker plots were generated, where rectangles show the first quartile, the median, and the third quartile. The two whiskers indicate the minimum and maximum values, and outliers are depicted as circles. For Gene Set Enrichment Analysis (GSEA) analysis, tumor samples were subdivided into top and bottom quartiles based on *LOXL2* expression and compared using GSEA, v4.0.3 (Broad Institute). Fragments Per Kilobase of transcript per Million (FPKM) mapped reads were analyzed using the Gene signatures (Hallmark gene sets, h.all.v7.1.symbold.gmt) from GSEA - Molecular Signature Database for Gene set enrichment analysis was used for pathway enrichment analysis with GSEA, with 1000 permutations and FDR<25% was considered statistically significant.

The dataset, patient subtypes and survival data from Bailey *et al.* were included in Supplementary Tables 14-16 of their published work[1]. To analyze the prognostic value of *LOXL2* mRNA expression, patients were stratified based on the median value of *LOXL2* and a survival analysis (Kaplan–Meier survival plot) was performed with R. LogRank test was used to determine statistical significance. Cox regression was used to calculate the hazard ratio.

A Pearson correlation of epithelial/mesenchymal specific gene expression with *LOXL2* expression was computed for the 179 PDAC patients included in the PDAC TCGA RNAseq database[2]. The correlation matrix was subjected to supervised hierarchical clustering and Euclidean distance measurement; average linkage clustering was applied. The heat map was generated using Morpheus provided by the Broad Institute.

Human cell cultures

To establish low-passage primary PDAC PDX-derived *in vitro* cultures, the indicated xenografts were minced, enzymatically digested with collagenase (Cat no. 07416, Stem Cell Technologies) for 60 min at 37°C and after centrifugation for 5 min at 500 × g, the cell pellets were resuspended and cultured in RPMI 1640 media (Invitrogen, Cat no. 61870044) containing 10% FBS (Invitrogen), 50 units/ml penicillin/streptomycin (Invitrogen, Cat no. 11548876) and fungizone (Invitrogen, Cat no. 15290018). Primary cultures were tested for Mycoplasma at least every 4 weeks. EGFP-labelled human PDAC cells were established by lentivirus transduction with an EGFP-expressing reporter lentiviral vector backbone (pRRL sin CMV IRES eGFP). sh*LOXL2*- and shSrc-expressing cells were established by lentivirus transduction with the previously-described[3] GFP-expressing lentiviral vectors from SuperArray. All lentiviruses used in this study were propagated as previously described in HEK293T

cells[4]. For lentivirus transduction of human PDAC cells, Panc354 or Panc253 cells were seeded on 6-well plates at a concentration of 3 to 5×10^4 cells/well. One ml of virus was directly overlaid on cells and polybrene (Cat no. 638133, Sigma) was added at a final concentration of 8 µg/ml. After 16 h, medium was changed. Stably transduced cells were obtained after GFP-positive cell sorting using a FACS Vantage SE Flow Cytometer and analyzed by BD FACSDiva software (BD Biosciences).

HEK293T were obtained from American Type Culture Collection (ATCC) and cultured as described above. To over express LOXL2, cells were transfected with a pcDNA3-flag vector encoding the mouse (NM_033325.2) Loxl2 or human (NM_002318.3) LOXL2 coding sequence (cds) as described[5]. These cells served as a positive control for the protein analyses described below.

Blood samples from healthy donors were provided by the BioBank Hospital Ramón y Cajal-IRYCIS (PT13/0010/0002), integrated in the Spanish National Biobanks Network (ISCIII Biobank Register No. B.0000678). Samples were processed following standard operating procedures with the appropriate approval of the Ethical and Scientific Committees (Control no. No. Control: DE-BIOB-73 AC65, RG.BIOB-57, and RG.BIOB-54), with informed consent and according to Declaration of Helsinki principles. Blood samples were diluted with PBS (Cat no.10010023, Gibco), overlayed on Ficoll (Cat no. L6115, Merck), and centrifuged at 400 × g for 40 min to isolate peripheral blood mononuclear cells (PBMC). PBMCs were cultured in the absence of serum for 24 h to allow monocytes to attach. Adherent monocytes were then cultured with RPMI 1640 media (Invitrogen, Cat no. 61870044) containing 10% FBS (Invitrogen), 50 units/ml penicillin/streptomycin (Invitrogen, Cat no. 11548876) and 1000U/ml M-CSF (R&D, Minneapolis, MN) for 7 to 10 days to allow for differentiation into M2 macrophages as previously described[6]. For macrophage conditioned media (MCM), polarized M2 macrophages were washed with 1X PBS and complete medium lacking M-CSF was added to the cultures and harvested 48 h later.

Microscopy, histology, histopathology and immunohistochemistry

For histopathological analysis, formalin-fixed, paraffin embedded (FFPE) blocks of human and/or mouse samples were serially sectioned (3 µm thick) and stained with hematoxylin and eosin (H&E). Additional serial sections were used for immunohistochemical (IHC) studies or for Picrosirious red staining. IHC primary antibodies, secondary antibodies and dilutions are detailed in Table S1. Surgically resected human PDAC tumors shown in Figure S1 have been previously described[6]. For IHC, antigens were visualized using 3,3-diaminobenzidine tetrahydrochloride plus (DAB+). Counterstaining was performed with hematoxylin. Human LOXL2 protein expression by IHC was performed on 2 µm FFPE tissue sections. After deparaffinization (60 °C for 40 min) and antigen-retrieval (Leica Bond ER Solution 2, pH 8.9-9.1 for 20 min), the LOXL2 primary antibody (1:200) was incubated for 20 min at RT followed the secondary-HRP antibody incubation. The staining was revealed by DAB standard Leica procedure.

In negative controls, the primary antibody was omitted. The rabbit polyclonal antisera against human LOXL2 was kindly provided by Dr. Csiszar and previously described [3 7 8]. The LOXL2 quantification was defined as positive when it was detected in at least 10% of tumor cells when compared with non-expression in normal tissue. To assess fibrillar collagen, FFPE sections of tumor tissues were stained with 0.1% picrosirious red (Sigma, Cat no. 141048.1610) and counterstained with Weigert's hematoxylin. Slides were digitalized with the Slide Scanner Axio Scan.Z1 (Carl Zeiss) and a 20X PlanApo objective (0.22 µm/pixel resolution) and analyzed with ZEN light (Carl Zeiss). Picrosirious red-stained sections were captured using polarized light and analyzed with Fiji package[9]. Fourier component analysis for directionality was performed on digitalized images using the Fiji plug-in "Directionality" (http://pacific.mpi-cbg.de/wiki/index.php/Directionality) to generate directionality plots. Analyses shown in Figure 7C were performed comparing wild-type [(+/+) KPC and HET KPC (KPC;Loxl2$^{+/-}$)] mice to KO KPC (KPC;Loxl2$^{-/-}$) mice or wild (+/+) KPC mice to KPCL2^{KI} [KPC;R26L2$^{+/KI}$ and KPC;R26L2$^{KI/KI}$] mice. Groups were only merged when no significant differences were observed between them.

For H&E-stained slides of pancreata, an in-house pathologist marked areas as normal tissue, ADM, PanIN or PDAC tumor tissue, which were compared to the total area to determine the percent of each. Moreover, tumors were classified as differentiated or poorly differentiated using the guidelines from the College of American Pathologists (https://documents.cap.org/protocols/cp-pancreas-exocrine-17protocol-4001.pdf). For macroscopic images of tumors or metastatic tissue, a Leica Stereomicroscope (MZ10F, Germany) with fluorescence was used, and images were captured with Leica LAS V4.8 software.

For IHC images acquired and analyzed in Figures 5D-E, S10, S11, S15 and S16A-B, sections (3-µm) were incubated with primary antibodies overnight at 4 °C followed by biotinylated secondary antibodies for 1h at room temperature (RT). Avidin-biotin peroxidase complex was applied according to the manufacturer's protocol (Vector Laboratories, CA). Slides were counterstained with hematoxylin and eosin. Quantification of stained slides was done by QuPath 0.2.3 (Bankhead, P. et al. (2017). QuPath: Open-source software for digital pathology image analysis. *Scientific Reports*. https://doi.org/10.1038/s41598-017-17204-5).

Primary mouse cell cultures

Established KPCL2^{KO} and KPCL2^{KI} cell lines were tested for Mycoplasma at least every 4 weeks. H2b-mCherry-labelled KPCL2^{KO} cells were established by lentivirus transduction of KPCL2^{KO} cells with a H2B-mCherry reporter lentiviral vector backbone, propagated as previously described in HEK293T cells[10]. For lentivirus transduction, KPCL2$^{-/-}$ ID90 cells were seeded on 6-well plates at a concentration of 3 to 5×10^4 cells/well. One ml of virus was directly overlaid on cells and polybrene (Cat no. 638133, Sigma)

was added at a final concentration of 8 µg/ml. After 16 h, medium was changed. Stably transduced cells were obtained after mCherry-positive cell sorting using a FACS Vantage SE Flow Cytometer and analyzed by BD FACSDiva software (BD Biosciences).

Murine bone-marrow-derived cells (BMDC) were isolated from the femur and tibiae of at least two mice by centrifugation. BMDC pellets were resuspended in RPMI 1640 media (Invitrogen, Cat no. 61870044) and cultured in the absence of serum for 24h to allow monocytes to attach. Adherent monocytes were then differentiated into macrophages under adherent conditions on non-tissue culture-treated 100mm dishes in RPMI supplemented with 10% FBS and 10ng/ml of murine M-CSF (Cat no. 315-02, PeproTech, London, UK). To polarize macrophages to M2, cultures were treated with 10 ng/ml of IL-4 (Cat no. 214-14, PeproTech) for 24h. For MCM, polarized M2 macrophages were washed with 1X PBS and complete medium lacking M-CSF was added to the cultures and harvested 48h later.

Patient serum samples and Enzyme linked immunosorbent assay (ELISA)

OSM levels in serum from PDAC patients and healthy donors and in conditioned media samples were determined using the OSM DuoSet Development kit (R&D, Cat no. DY295) as per the manufacturer's instructions.

MCM, recombinant TGFß and OSM experiments

For induction of EMT, indicated cells were seeded in 6-well plates and treated with 100 ng/ml of recombinant human OSM (no. PHC5015, Thermo Fisher Scientific), 200 ng/ml of recombinant mouse Osm (Cat. no 495-MO-025; R&D), 5 ng/ml of recombinant human TGFß1 (Cat no. 100-21, Peprotech) or 2ml of MCM. Treatments and MCM were replaced daily for the duration of the experiment. After indicated time points, cells were photographed with an EVOS FL microscope (Thermo Fisher Scientific) using a 10X objective with phase contrast and cells and/or media were harvested for further analyses, including WB analysis, RT-qPCR, or ELISA.

RNA Preparation and Real-Time quantitative PCR

Total RNA from human PDX-derived cell lines and murine PDAC tumors and cell lines was isolated by the guanidine thiocyanate (GTC, VWR AMRESCO Chemicals, Cat no. K965-250ML) method using standard protocols[11]. RNA from the surgically resected human PDAC tumors (n=30) shown in Figure 1B have been previously described[6]. RNA from normal pancreas was purchased from ThermoFisher Scientific (Cat no. QS0621) and Quimigen (Cat no. R1234188-P). RNA extraction from formalin-fixed paraffin-embedded (FFPE) sections was performed using the PureLink™ FFPE RNA Isolation Kit (ThermoFisher Scientific, Cat. no. K156002). Total RNA was extracted from 10 slices of 10 µm-thick FFPE sections.

For cDNA synthesis, 1 microgram of purified RNA was reverse-transcribed using the Thermo Scientific Maxima First Strand cDNA Synthesis Kit (ThermoFisher Scientific, Cat no. K1672) according to manufacturer´s instructions, followed by SYBR green RT-qPCR (PowerUp™ SYBR™ Green Master Mix, ThermoFisher Scientific, Cat no. A25777) using an Applied Biosystems StepOnePlus™ real-time thermocycler (ThermoFisher Scientific). Thermal cycling consisted of an initial 10 min denaturation step at 95 °C followed by 40 cycles of denaturation (15 sec at 95 °C) and annealing/extension (1 min at 60 °C). mRNA copy numbers were determined relative to standard curves comprised of serial dilutions of plasmids containing the target coding sequences and normalized to ß-actin or HPRT levels, as indicated. Species-specific primers used are listed in Table S2.

Western blot analysis

Tumors, PDXs or cells were harvested in RIPA buffer (Sigma, Cat no. R0278-50ML) supplemented with a protease inhibitor cocktail (Roche Applied Science, Indianapolis, IN). Tumors and PDXs were mechanically digested. Cell supernatants were concentrated using the Millipore Centriplus centrifugal concentrator 50kDA (Cat. no. 4423), as per the manufacturer's instructions. Fifty to 80 µg of protein or 30 µl of concentrated media were resolved by SDS-PAGE and transferred to Amersham™ Hybond® P Western blotting PVDF membranes (Sigma, Cat no. 10600021). Membranes were sequentially blocked with 1X TBS containing 5% BSA (w/v) and 0.5% Tween20 (v/v), incubated with a 1:500-1:5000 dilution of indicated antibodies (see Table S1) overnight at 4ºC, washed 5 times with 1X TBS containing 0.5% Tween20 (v/v), incubated with horseradish peroxidase-conjugated goat anti-rabbit or goat anti-mouse antibody (Amersham), and washed again to remove unbound antibody. Bound antibody complexes were detected with SuperSignal chemiluminescent substrate (Pierce, Cat no. 34580) and images were obtained using the MyECL or iBright Imager (Thermo Fisher Scientific). Densitometric ratios were determined using ImageJ software and by measuring the intensity of each band and normalizing to total protein (i.e., Ponceau S, Sigma, Cat. no. P7170) or a specific housekeeping loading control.

The specificity of the anti-human/mouse-LOXL2 antibody for WB was validated using lysates from HEK239T cells transiently transfected with a plasmid (pcDNA3-Flag) expressing the full cds of murine or human LOXL2.

Migration assay

Invasion assays were performed using 8.0 µm transparent PET membrane trans-well chambers (Cat no. 353097, Falcon). 1×10^5 human PDX-derived cells or mouse PDAC-derived cells, cultured with control media, MCM for 48h or pretreated with OSM or TGFß1 (concentrations detailed above), were added to the top of the insert, and 750 µl of complete DMEM/F12 media supplemented with 20% FBS, or RPMI media supplemented with 2%, 10% or 50% FBS was added to the lower chamber. The assay

chambers were incubated for 18h at 37°C. Invaded cells were fixed in 4% PFA and stained with Diff Quik (Cat. no. WS32-1L, Sigma) or Crystal violet (Sigma, Cat no. C3886-100G), and the number of cells that migrated through to the lower chamber were counted for Diff Quik-stained cells or optically measured (i.e., optical density) following incubation with 1X PBS containing 1% SDS.

Wound healing assay

Human PDX-derived cells were cultured until confluence and then wounded using a 200 µl yellow pipette tip. Cells were treated with 100 ng/ml of rOSM 24h prior to wounding. Three wounds were made for each sample, and migration distance was photographed and measured at time 0h and 12h.

Sphere formation assay

Pancreatic CSC spheres were generated by culturing primary pancreatic cancer cells (2,000-10,000 cells/ml) in ultra-low attachment plates (Corning) using serum-free DMEM/F12 (Invitrogen, Cat no. 21331046) supplemented with B27 1:50 (Invitrogen, Cat no. 17504044), 20 ng/mL bFGF (PAN-Biotech, Sigma, Cat no. GF446-10UG), L-Glutamine (Invitrogen, Cat no. 25030081), 50 units/ml penicillin/streptomycin (Invitrogen, Cat no. 11548876) and fungizone (Invitrogen, Cat no. 15290018). Seven days later, spheres were counted with an inverted EVOS FL microscope (Thermo Fisher Scientific) using a 10X objective with phase contrast. Sphere counts are represented as the no. of spheres/ml.

Colony assay

For colony formation assays, 500 cells were seeded in 24-well plates. Cells were cultured in RPMI 1640 containing 10% FBS at 37°C, 5% CO2. After 5-10 days, cells were fixed with PFA 4% (Paraformaldehyde, 16% w/v aq. soln., methanol free, Alfa Aesar™, Cat no. 11400580) for 10min, washed with PBS and stained with Crystal violet (Sigma, Cat no. C3886-100G) for 1h. Wells were digitalized and the percent of colonies/total areas was determined with Fiji package.

Flow cytometry

Cells were resuspended in Flow buffer [1X PBS; 3% FBS (v/v); 3mM EDTA (v/v)] before analysis with a 4-laser Attune™ NxT Acoustic Cytometer (Thermo Fisher Scientific). Explanted lungs and livers were digested with Collagenase P (11213857001, Roche), to obtain single cell suspensions. Briefly, tissues were minced using a scalpel and forceps and transferred to a 50ml conical tube. 500ml of FBS-free medium and 500 µl of Collagenase P 1x (0.2mg/ml) (diluted in HBSS) were added to the tubes. Samples were incubated for 15 min at 37°C, vortexing every 5 min. After incubation, digestions were stopped by adding 1 mL of HBSS containing 10% FBS. Tubes were centrifuged for 5 min at 1500 rpm and supernatants were removed. ACK lysis buffer was used to remove erythrocytes by incubating samples for 5 min at room temperature HBSS was then added, and samples were centrifuged, supernatant

removed and cell pellets resuspended in flow cytometry buffer (PBS with 2%FBS and 3 mM EDTA). For analysis of murine cells, cell suspensions were blocked with anti-mouse CD16/CD32 Purified (Cat no. 14-0161, Thermo Fisher Scientific) and normal mouse serum (Cat no. 24-5544, Thermo Fisher Scientific) to block Fc receptors. For cell surface marker expression, refer to antibodies listed in Table S1. For all assays, 2mg/ml DAPI (4',6-diamidino-2-phenylindole, Sigma, Cat no. D9542-5MG) was used to exclude dead cells. Data were analyzed with FlowJo 9.3 software (Tree Star Inc., Ashland, OR). For the MAM cytometry experiments shown in Figure 7A, analyses were performed comparing [wild-type (+/+) KPC and HET KPC (KPC;Loxl2$^{+/-}$)] mice to KO KPC (KPC;Loxl2$^{-/-}$) mice or wild (+/+) KPC mice to KPCL2^{KI} [KPC;R26L2$^{+/KI}$ and KPC;R26L2$^{KI/KI}$] mice. Groups were only merged when no significant differences were observed between them.

For the detection of H2B-mCherry KPCL2^{KO} and EGFP KPCL2^{KI} cells in blood samples, the Attune™ NxT No-Wash No-Lyse Filter Kit (Cat no. 100022776, Thermo Fisher Scientific) was used to efficiently detect nucleated mCherry or EGFP in blood samples without RBC lysing or washing. Data were analyzed with FlowJo 9.3 software (Tree Star Inc., Ashland, OR). For the detection of H2B-mCherry KPCL2^{KO} and EGFP KPCL2^{KI} in indicated organs, tissues were processed as described above.

In vivo tumorigenicity and metastasis assays

NOD-SCID and C57Bl/6 mice were purchased from our in-house breeding facility (Instituto de Investigaciones Biomédicas **"**Alberto Sols**"** CSIC-UAM). For liver metastasis assays using human PDX-derived cells, 8-week-old NOD-SCID mice (Instituto de Investigaciones Biomédicas **"**Alberto Sols**"** CSIC-UAM) were injected intrasplenically with 1×10^5 Panc354 cells pretreated in vitro for 48h with Ctl or M2-polarized macrophage conditioned media (MCM). Mice were sacrificed 10 weeks post injection and macroscopic liver metastases were determined. For lung colonization assays, 8-week-old NOD-SCID mice were injected intravenously via the tail vein with 2.5×10^5 EGFP-expressing Panc354 or Panc253 cells pretreated 5 days with control or MCM, or 1×10^6 KPCL2^{KO} or KPCL2^{KI} cells (resuspended in 100 µl 0.9% physiological saline solution) using a 27-G needle. Lungs were harvested 2- or 4-weeks post injection (as indicated), photographed, weighed, fixed in 4% PFA overnight at 4 °C and subsequently paraffin embedded. For images presented in Figure 6A-B, when tumor cells where present in a vascular space lined with endothelium it was deemed intravasation. To determine the percentage of EGFP positive Panc354 or Panc253 cells, lungs were digested with Collagenase P (11213857001, Roche) and EGFP was determined by flow cytometry using an Attune NxT Acoustic Cytometer (ThermoFisher Scientific).

For in vivo tumorigenicity assays using murine PDAC cells, serial dilutions of KPCL2^{KO} or KPCL2^{KI} cell lines in Matrigel^{TM} (Cat no. 356234, Corning) were subcutaneously injected into 8-week-old female

nude mice (Hsd:Athymic Nude-Foxn1nu/Foxn1+; Envigo) and tracked for 14 weeks for tumor formation. At the time of sacrifice, tumors were extracted, photographed and weighed.

For orthotopic experiments, 2.5×10^5 H2b-mCherry-labelled KPCL2^{KO} or EGFP+ KPCL2^{KI} cells, alone or at a 1:1 ratio, were resuspended in 50 µl Matrigel™ (Cat no. 356234, Corning) and slowly injected into the pancreas of 8-week-old NOD-SCID mice. Mice were sacrificed 4 weeks post infection, blood was collected in Vacutest® EDTA tubes (VWR, Cat no. KIMA135300) and analyzed as described above, and pancreata and livers were excised, photographed, weighed, digested as detailed above using Collagenase P (11213857001, Roche) and the percentage of mCherry and/or EGFP-positive cells were determined by flow cytometry using an Attune NxT Acoustic Cytometer (ThermoFisher Scientific).

Syngeneic orthotopic experiments were performed in C57Bl/6 mice as described above; however, murine PDAC tumor pieces [derived from a backcrossed KPC mouse[12]] of approximately 20 mm^3 were orthotopically implanted into the pancreas in lieu of a cell suspension. For macrophage depletion, mice received 150 µl of clodronate-encapsulated liposomes (ClodronateLiposomes, Amsterdam, Netherlands) via retro-orbital injection twice per week, beginning 24h prior to orthotopic tumor implantation and lasting throughout the course of the experiment. At sacrifice, pancreata, livers and lungs were excised, photographed, weighed, fixed in 4% PFA overnight at 4°C and subsequently paraffin embedded. A macroscopic inspection for metastases was performed.

SUPPLEMENTARY TABLES

Table S1. Antibodies

1ª Abs-Epitope	Source	Dilution	Application	Manufacturer (Catalog no.)
α-hu/mu-β-ACTIN	Mouse monoclonal	1:5000	WB	ThermoFisher (MA1-140)
α-hu-TUBULIN	Mouse monoclonal	1:5000	WB	Elabscience (E-AB-20033)
α-hu/mu-LOXL2	Rabbit	1:1000	WB	Abcam (ab179810)
α-hu-phospho-STAT3	Rabbit	1:500	WB	Cell Signalling (9145)
α-hu-STAT3	Mouse monoclonal	1:500	WB	BD (610189)
α-hu-LOXL2	Rabbit polyclonal antisera	1:200	IHC	kindly provided by Dr. Csiszar and previously described [3 7 8]
α-ms-GAPDH	Mouse monoclonal	1:5000	WB	Abcam (ab8245)
α-ms-EpCAM-FITC; or -EpCAM-PE	Rat	1:100; 1:50	FC	FITC (BioLegend, 118208, BioLegend 118202; PE (Miltenyi, 130-102-265)
α-ms-CD133 APC	Rat	1:10	FC	Miltenyi (130-102-19)
α-ms-CD11b PerCP Cy5.5	Rat	1:200	FC	TONBO Bioscience (65-0112)
α-ms-F4/80-PE	Mouse monoclonal	1:100	FC	MIltenyi (130-102-422)
α-ms-Vimentin	Mouse	1:200	IHC	Abcam (ab8978)
α-ms-Twist	Rabbit	1:100	IHC	Abcam (ab49254)
α-ms-ß-Catenin	Rabbit	1:200	IHC	Cell Signalling (9562)
α-ms-Snail1	Rabbit	1:100	IHC	Abcam (ab180714)
α-ms-Zeb1	Rabbit	1:500	IHC	Bethyl (A301-922A-T)
α-ms-CD3	Rabbit	1:100	IHC	DAKO (A0452)
α-ms-F4-80	Rat	1:100	IHC	Invitrogen (MF-48000)
α-ms-CD206	Goat	1:150	IHC	R&D (AF2535)
α-ms-E-cadherin	Mouse	1:100	IHC	BD Pharmingen (610181)
α-ms-pStat3	Rabbit	1:100	IHC	Cell Signaling (CS9145)
α-ms-pFAK	Rabbit	1:200	IHC	Thermo (900255)
α-ms-pMLC2	Rabbit	1:200	IHC	Cell Signaling (CS3674)
α-ms-CD3	Rabbit	1:100	IHC	DAKO (A0452)

2ª Abs-Epitope	Source	Dilution	Application	Manufacturer (Catalog no.)
Anti-mouse-HRP	Sheep	1:5000	WB	Amersham (NA931)
Anti-rabbit-HRP	Donkey	1:5000	WB	Amersham (NA934)

Table S2. RTqPCR primer sequences

Gene	Species	Primer sense	Primer antisense
β-ACTIN	human	GCGAGCACACGAGCCTCGCCTT	CATCATCCATGGTGAGCTGGCGG
SNAIL1	human	CTCCCTGTCAGATGAGGAC	CCAGGCTGAGGTATTCCTTG
SNAIL2	human	GGGGAGAAGCCTTTTTCTTG	TCCTCATGTTTGTGCAGGAG
VIMENTIN	human	GAGAACTTTGCCGTTGAAGC	GCTTCCTGTAGGTGGCAATC
ZEB1	human	CCAGGTGTAAGCGCAGAAA	CCACAATATGCAGTTTGTCTTCA
CDH1	human	TGCCCAGAAAATGAAAAAGGC	GTGTATGTGGCAATGCGTTC
ZEB2	human	GAGCAGGTAATCGCAAGTTCAA	CACTCGTAAGGTTTTTCACCACTGT
LOX	human	GCATACAGGGCAGATGTCAG	GTGTTGGCATCAAGCAGGTC
LOXL1	human	AGCATCCACTTATGTGCAGAGA	GAGGAAGTCTGCTGTGCCCT
LOXL2	human	GGCACCGTGTGCGATGACGA	GCTGCAAGGGTCGCCTCGTT
LOXL3	human	AGAGGCCACAGGCTGGACCC	GCCCCGGGAGGCACATTCAG
LOXL4	human	TGACTTTCGTCCAAAGACTGG	TTGGAGCCATTGAGAGTGAG
β-actin	mouse	TGGAATCCTGTGGCATCCATGAAAC	TAAAACGCAGCTCAGTAACAGTCCG
Hprt	mouse	TCCTCCTCAGACCGCTTTT	CCTGGTTCATCATCGCTAATC
Lox	mouse	CCTTCAGCCACTCTCCTCTG	GCACAGCTGTCACCAACATT
Loxl1	mouse	GCCAGTGGATCGACATAACTG	ACAATGTACTTGGGGTTCACG
Loxl2	mouse	TGACTGCCAGTGGATAGACATC	GTTGGGGTTAATGACAACCTG
Loxl3	mouse	ATCCACAACCTAGGAAGAGCTG	TGGTAATGCCCATGACACTC
Loxl4	mouse	GGTTGCACAACTGCCACA	GGGAGTGCAGTAATGGCTT
Zeb1	mouse	TGAGCACACAGGTAAGAGGCC	GGCTTTTCCCCAGAGTGCA
Snail1	mouse	CTTGTGTCTGCACGACCTGT	CTTCACATCCGAGTGGGTTT
Twist	mouse	AGCTACGCCTTCTCCGTCT	TCCTTCTCTGGAAACAATGACA
Pdgfb	mouse	GCGTATCTATATCTTTGTGCCAGA	ACAGGTCCTCGGAGTCCAT
Sparc	mouse	AGAGGAAACGGTCGAGGAG	CTCACACACACCTTGCCATGTT
S100a4	mouse	GGAGCTGCCTAGCTTCCTG	TCCTGGAAGTCAACTTCATTGTC
MCol6A	mouse	GCAAGGATGAGCTGGTCAA	GTCCACGTGCTCTTGCATC
Cdh1	mouse	CCCGGGACAATGTGTATTACTATGA	GCAGCTGGCTCAAATCAAAGTCC

SUPPLEMENTARY REFERENCES

1. Bailey P, Chang DK, Nones K, et al. Genomic analyses identify molecular subtypes of pancreatic cancer. *Nature* 2016;531(7592):47-52.
2. Salt MB, Bandyopadhyay S, McCormick F. Epithelial-to-mesenchymal transition rewires the molecular path to PI3K-dependent proliferation. *Cancer Discov* 2014;4(2):186-99.
3. Moreno-Bueno G, Salvador F, Martin A, et al. Lysyl oxidase-like 2 (LOXL2), a new regulator of cell polarity required for metastatic dissemination of basal-like breast carcinomas. *EMBO Mol Med* 2011;3(9):528-44.
4. Sainz B, Jr., Barretto N, Martin DN, et al. Identification of the Niemann-Pick C1-like 1 cholesterol absorption receptor as a new hepatitis C virus entry factor. *Nat Med* 2012;18(2):281-5.
5. Peinado H, Del Carmen Iglesias-de la Cruz M, Olmeda D, et al. A molecular role for lysyl oxidase-like 2 enzyme in snail regulation and tumor progression. *EMBO J* 2005;24(19):3446-58.
6. Sainz B, Jr., Alcala S, Garcia E, et al. Microenvironmental hCAP-18/LL-37 promotes pancreatic ductal adenocarcinoma by activating its cancer stem cell compartment. *Gut* 2015;64(12):1921-35.
7. Fong SF, Dietzsch E, Fong KS, et al. Lysyl oxidase-like 2 expression is increased in colon and esophageal tumors and associated with less differentiated colon tumors. *Genes Chromosomes Cancer* 2007;46(7):644-55.
8. Barry-Hamilton V, Spangler R, Marshall D, et al. Allosteric inhibition of lysyl oxidase-like-2 impedes the development of a pathologic microenvironment. *Nat Med* 2010;16(9):1009-17.
9. Schindelin J, Arganda-Carreras I, Frise E, et al. Fiji: an open-source platform for biological-image analysis. *Nat Methods* 2012;9(7):676-82.
10. Valle S, Alcala S, Martin-Hijano L, et al. Exploiting oxidative phosphorylation to promote the stem and immunoevasive properties of pancreatic cancer stem cells. *Nat Commun* 2020;11(1):5265.
11. Chomczynski P, Sacchi N. Single-step method of RNA isolation by acid guanidinium thiocyanate-phenol-chloroform extraction. *Anal Biochem* 1987;162(1):156-9.
12. Hingorani SR, Wang L, Multani AS, et al. Trp53R172H and KrasG12D cooperate to promote chromosomal instability and widely metastatic pancreatic ductal adenocarcinoma in mice. *Cancer Cell* 2005;7(5):469-83.

SUPPLEMENTARY FIGURES AND FIGURE LEGENDS

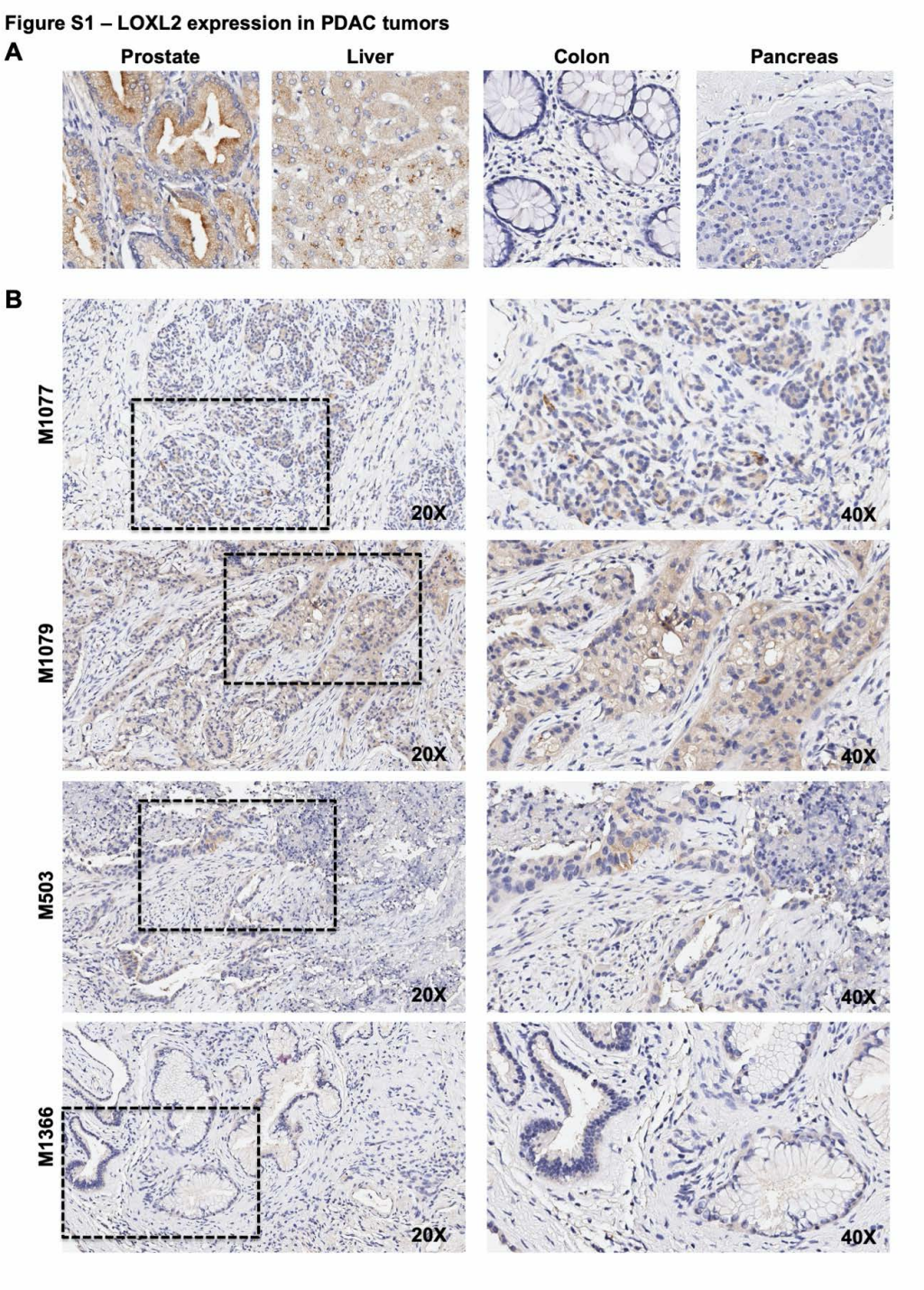

Figure S1: LOXL2 expression in PDAC tumors.
(A-B) Representative immunohistochemical staining for LOXL2 expression in sections from (A) normal prostate, liver, colon or pancreatic tissue or (B) PDAC samples analyzed in Fig 1B. 20X magnification. Insets indicate area that is shown on the right at 40X.

Figure S2 – GSEA of pathways enriched in patients with high *LOXL2* mRNA levels

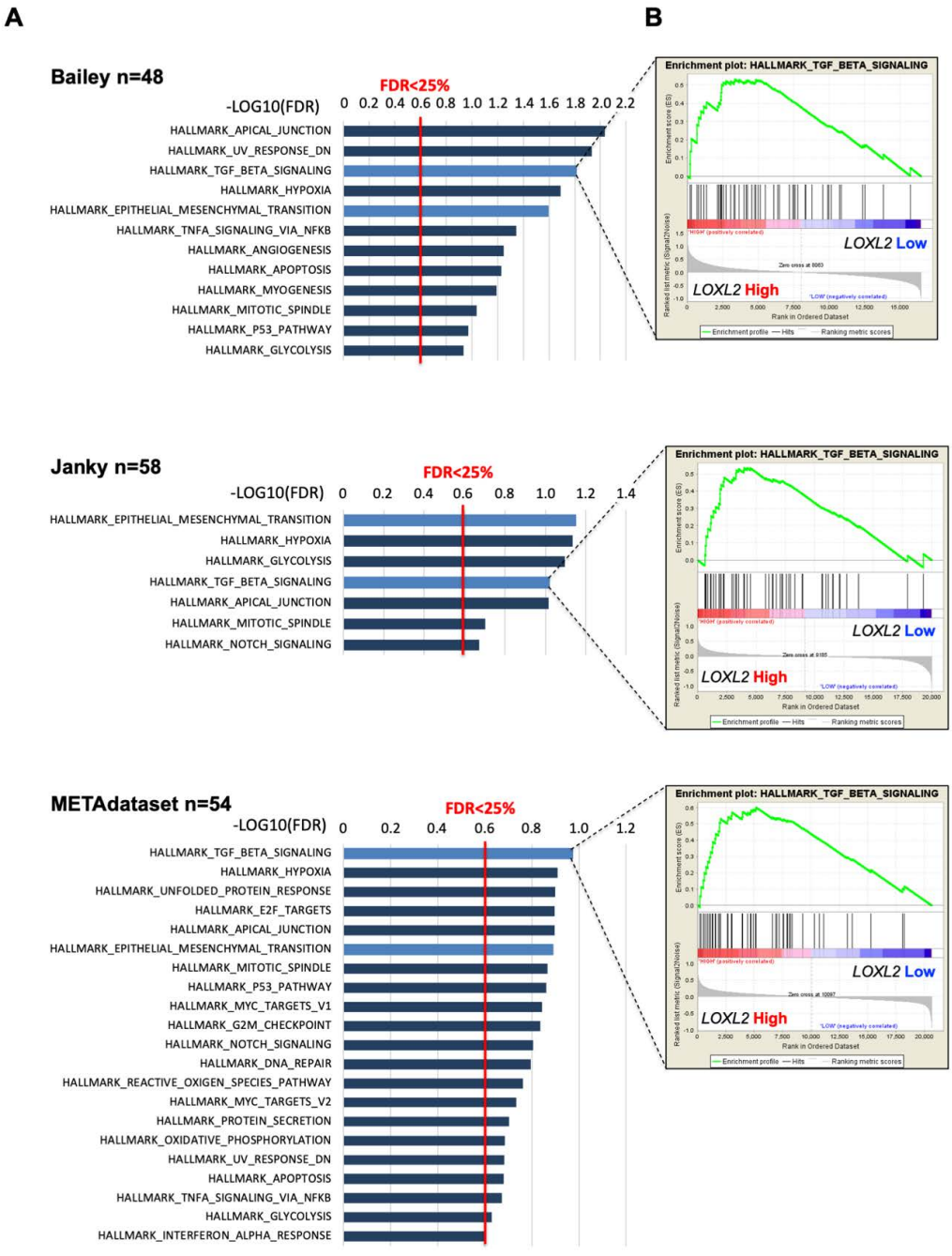

Figure S2: GSEA of pathways enriched in patients with high *LOXL2* mRNA levels.
(A) Pathways enriched in the transcriptional profiles of tumors belonging to the top *LOXL2* high expression quartile group, compared with the bottom expression quartile group in the Bailey, Janky or META datasets. A nominal p value of <0.05, FDR<25% is considered statistically significant. Shown are the –log10 (FDR) values for each pathway using the Hallmark genesets.
(B) Example enrichment plots for TGFß signaling pathways from the indicated datasets.

Figure S3 – *LOXL2* mRNA levels correlate with EMT, disease stage and survival parameters

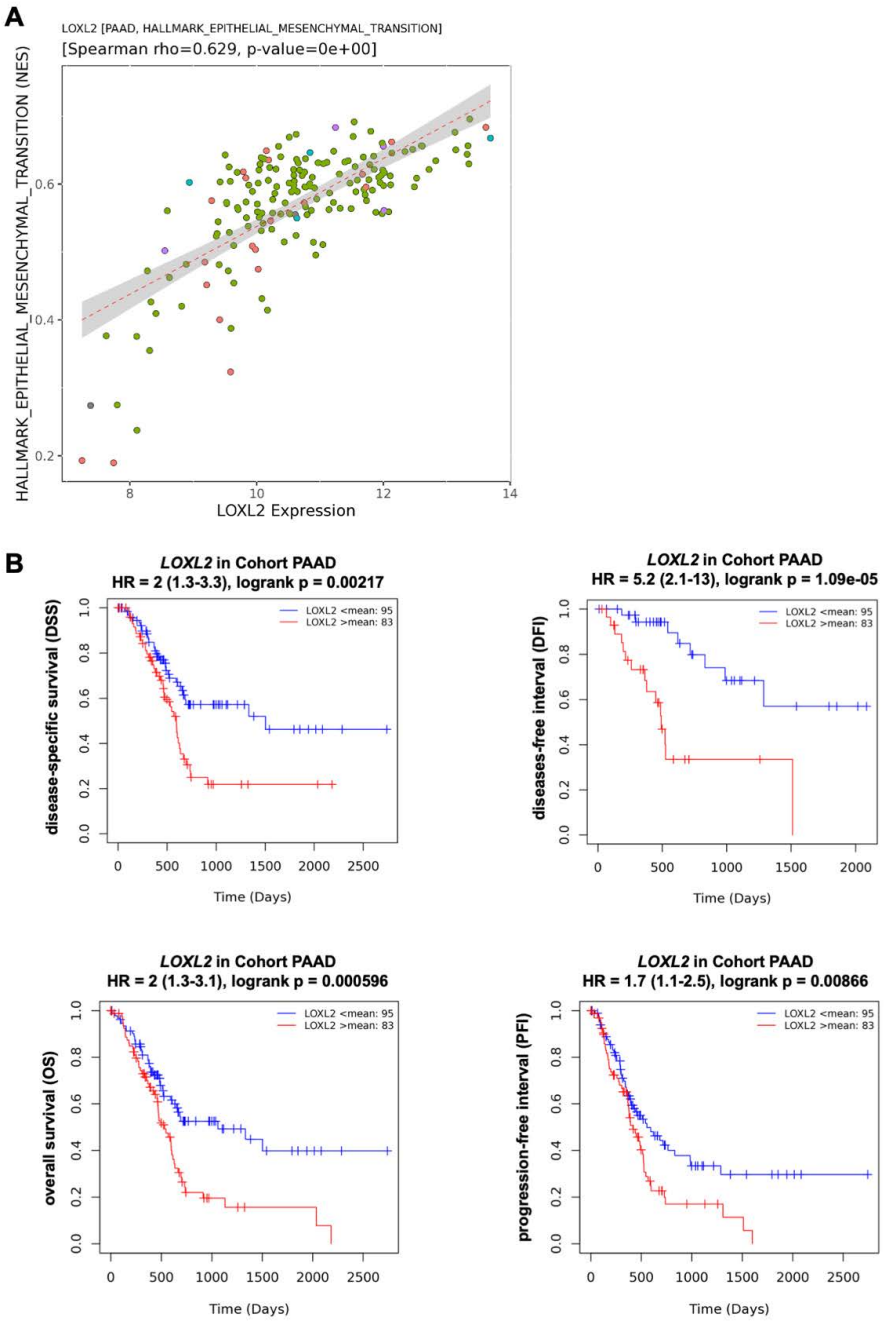

Figure S3: *LOXL2* mRNA levels correlate with EMT, disease stage and survival parameters.
(A) Scatter Plot showing correlation between *LOXL2* mRNA levels and EMT-related genes (Hallmarks EMT) in TCGA-PAAD dataset (n=185) curated by EMTome. (Spearman's ρ=0.629, p=0.000)
(B) *LOXL2* mRNA levels correlate with disease-specific survival (DSS) (HR=2, logrank p=0.00217), diseases-free interval (DFI) (Hazard ratio (HR)=5.2, logrank p=1.09e-05), overall survival (OS) (HR=2, logrank p=0.000596) and progression-free interval (PFI) (HR=1.7, logrank p=0.00866), curated by EMTome (http://www.emtome.org).

Figure S4 – MCM or OSM promote metastasis and EMT in PDAC PDX-derived cells

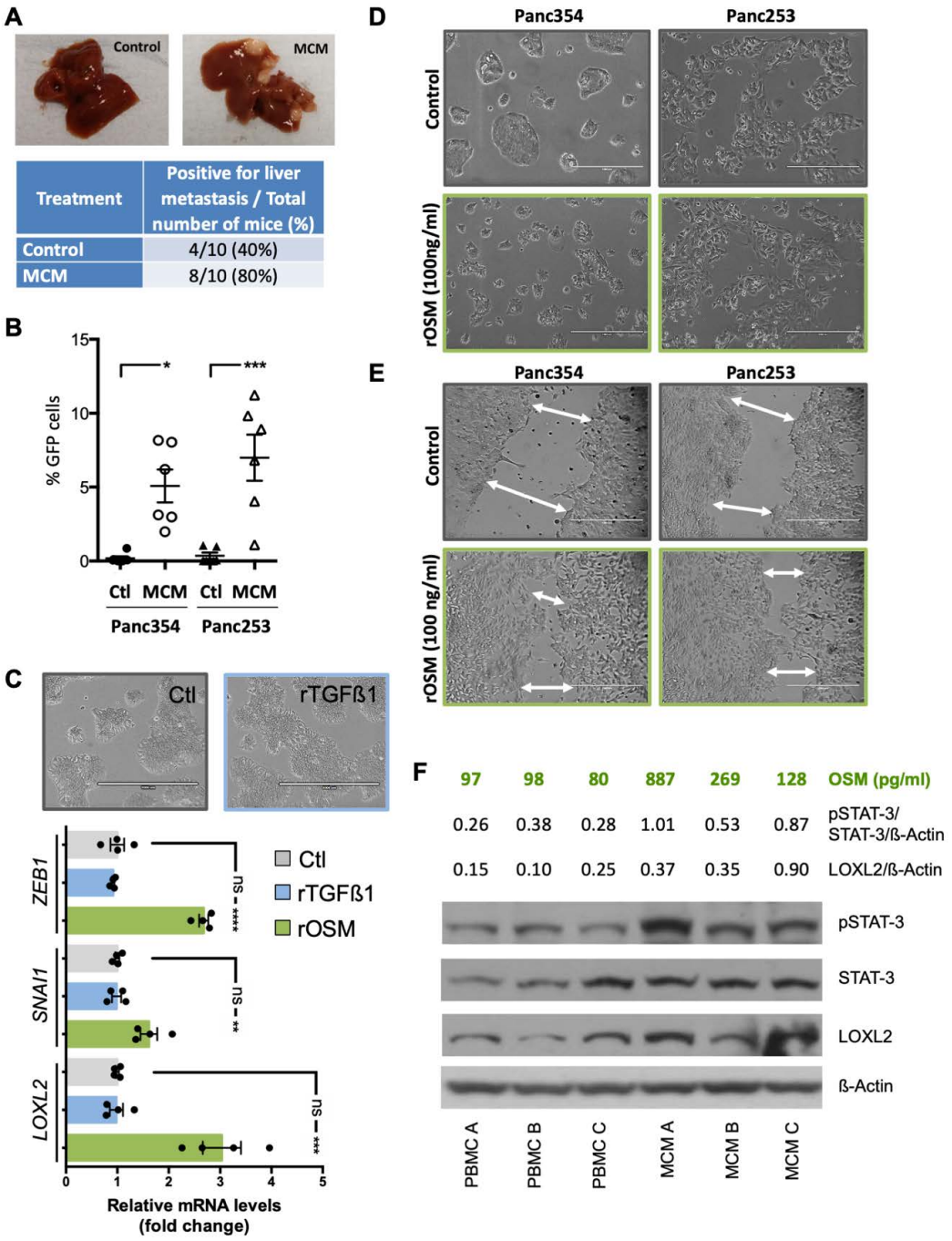

Figure S4: MCM or OSM promote metastasis and EMT in PDAC PDX-derived cells.

(A) Representative images of liver metastasis in NOD-SCID mice injected intrasplenically with 1×10^5 Panc354 cells pre-treated for 48 h with Ctl or M2-polarized macrophage conditioned media (MCM) in vitro and then injected in vivo. (top) Livers were collected and imaged for macrometastases. (bottom) Summary of the number of mice with macrometastases / number of mice injected.

(B) GFP-expressing Panc354 and Panc253 cells were pre-treated for 5 days with control media or MCM, and then 2×10^5 pre-treated cells were resuspended in 100µl physiological saline and tail vein injected into NOD-SCID mice (*n* = 6 mice per group). Lungs were harvested 2 weeks post injection and the percentage of GFP-positive cells

was determined by flow cytometry. Shown are the mean percent of GFP positive cells ± SEM within the single cell, live and debris-free population for each digested lung (* p<0.05, *** p<0.001, as determined by two-sided t test with Mann Whitney u test).

(C) Human Panc354 PDX-derived cells were cultured for 72h with control media (Ctl), recombinant (r) TGFß1 (5ng/ml) or rOSM (100ng/ml). (top) Representative images of control- and rTGFß1-treated cells. Scale bar = 400µm. (bottom) Mean fold-change ± SD of relative mRNA levels for the indicated target genes in Ctl-, rTGFß1 or rOSM-treated PDX-derived cells. Values were normalized to ß-actin levels and Ctl-treated samples were set as 1.0. (* $p < 0.05$, ** $p < 0.01$, *** $p < 0.001$, ns = not significant, determined by one-way ANOVA with Dunnett post-test, comparing rTGFß1 and rOSM to Ctl).

(D-E) Human Panc354 and Panc253 PDX-derived cells were cultured for 72h with control media or rOSM (100ng/ml). (D) Representative images of control- and rOSM-treated cells. (E) Representative images from wound healing assay for Control-treated or rOSM-treated cells 12 h following wound initiation. Scale bar = 400µm.

(F) Western blot analysis of pSTAT3, total STAT-3 and LOXL2 in human Panc354 PDX-derived cells following treatment for 72h with media from unpolarized PBMCs or conditioned media (CM) from M2-polarized macrophages, from 3 donors (A, B and C). Levels of OSM present in each CM was determined by ELISA and is indicated above as pg/ml. Densitometric ratios for indicated proteins are shown. ß-actin served as a loading and densitometry normalization control.

Figure S5 – *LOXL2* is not necessary for OSM- or MCM-mediated EMT

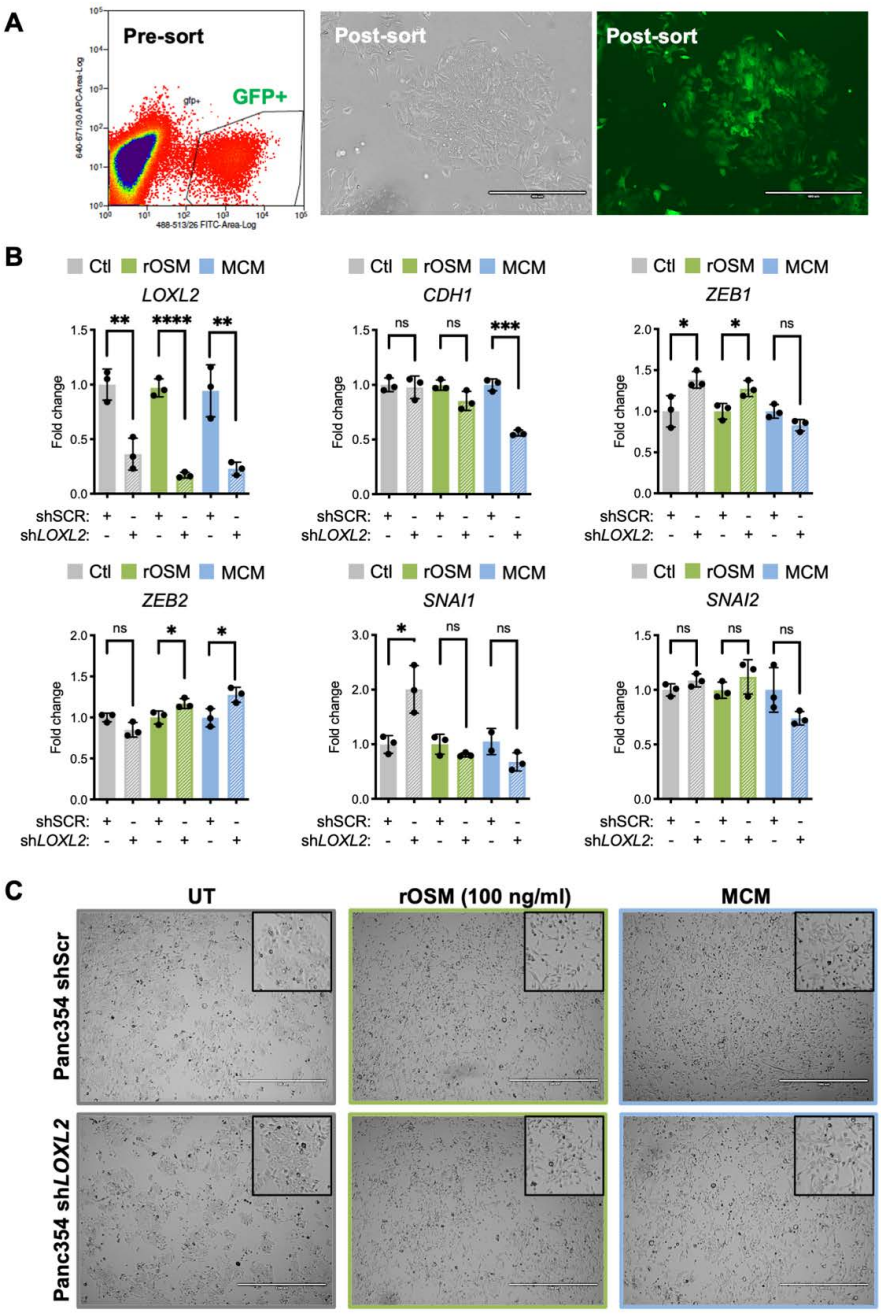

Figure S5: *LOXL2* is not necessary for OSM- or MCM-mediated EMT.
(A) Flow cytometry dot plot analysis of human Panc354 cells 48h post-infection with an sh*LOXL2* GFP-expressing lentiviral vector and prior to sorting for GFP (left), and the same cells 5 days post-sorting: light field (middle) and fluorescence (right). Scale bar = 400µm.
(B-C) Human Panc354 cells, stably transfected with an shScr GFP- or sh*LOXL2* GFP-expressing lentiviral vector were cultured for 72h with control media (Ctl), recombinant (r) rOSM (100ng/ml) or MCM. (B) Mean fold-change ± SD in relative mRNA levels for the indicated target genes in Ctl-, rOSM- or MCM-treated shScr or sh*LOXL2* cells. Values were normalized to ß-actin levels and shSrc cultures were set as 1.0 for all treatments (ns = not significant, * $p < 0.05$, ** $p < 0.01$, *** $p < 0.001$, **** $p < 0.0001$, as determined by unpaired Student's t test). (C) Representative images of cells 72h post treatment. Scale bar = 1000µm. Inset = 4X amplification.

Figure S6 – MCM, TGFß1 and OSM promote Loxl2 expression in murine PDAC-derived cells

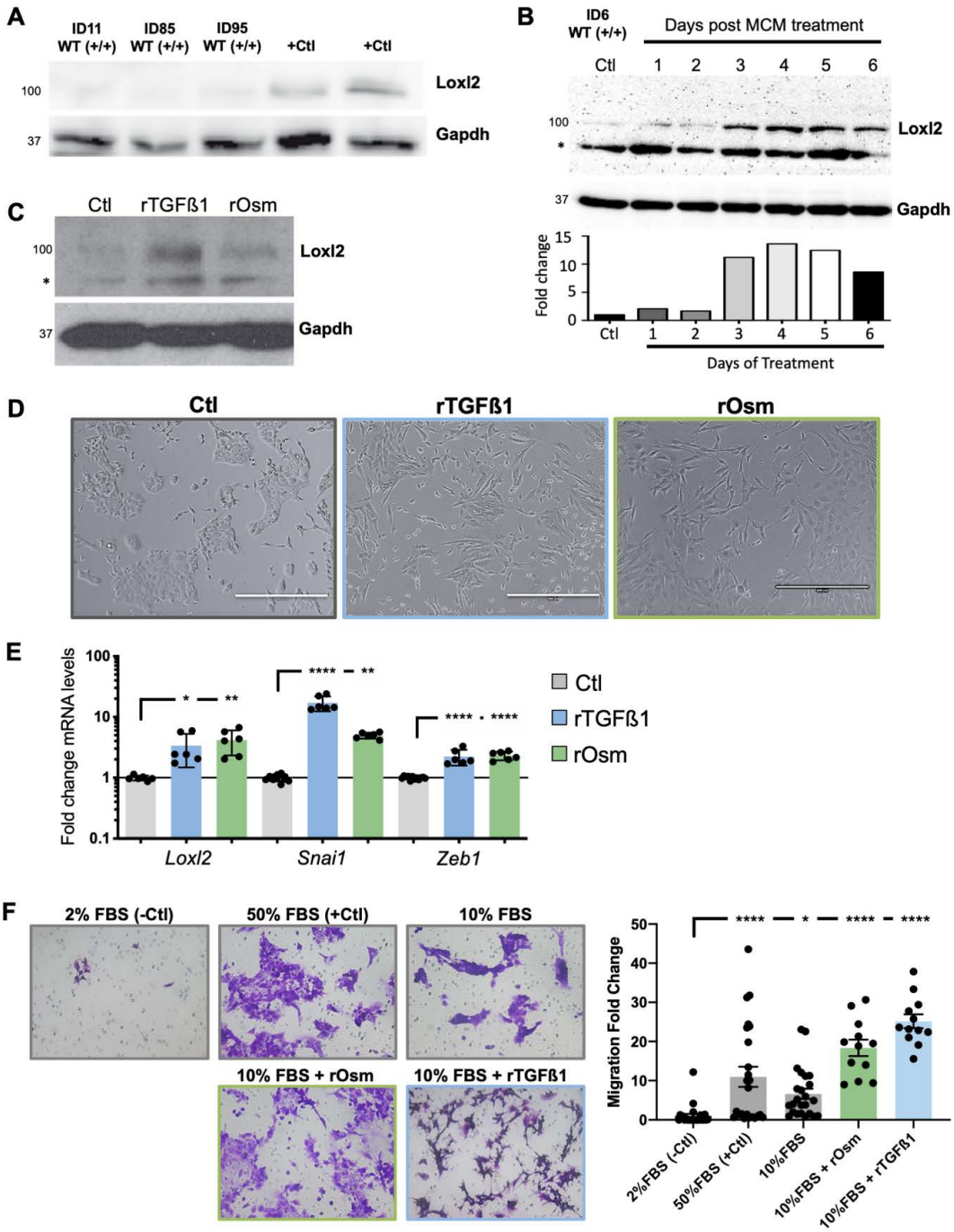

Figure S6: MCM, TGFß1 and Osm promote Loxl2 expression in murine PDAC-derived cells.
(A) Western blot analysis of Loxl2 expression in cell lysates from the indicated three murine KPC PDAC-derived wt (+/+) cell lines (ID11, ID85 and ID95). Gapdh, loading control. Positive control (+Ctl) = cell lysate from murine Loxl2 overexpressing 293T cells.
(B) Murine KPC PDAC-derived ID6 cells were untreated (Ctl) or cultured for 6 days with M2-polarized murine macrophage conditioned media (MCM). (top) Western blot analysis of murine Loxl2 expression over the course of 6 days. Gapdh served as a loading and densitometry normalization control (bottom). * = non-specific band.

(C-E) Murine KPC PDAC-derived cells were untreated (Ctl) or cultured for 72h with rTGFß1 (5ng/ml) or rOsm (100-200ng/ml). (C) Western blot analysis of murine Loxl2. Gapdh served as a loading control. * = non-specific band. (D) Representative images of Ctl and treated cells. Scale bar = 400µm. (E) Mean fold-change ± SD of relative mRNA levels for the indicated target genes in untreated (Ctl), rTGFß1- or rOsm-treated murine KPC PDAC-derived cells (ID11, ID85 and ID95). Values were normalized to ß-actin levels and Ctl-treated samples were set as 1.0. (*n*=2 technical replicate values per cell line, * $p < 0.05$, ** $p < 0.01$, **** $p < 0.0001$, as determined by one-way ANOVA with Dunnett post-test, comparing rTGFß1 and rOsm to Ctl).

(F) Murine KPC PDAC-derived ID95 cells were untreated or cultured for 72h with rTGFß1 (5ng/ml) or rOsm (200ng/ml). Left, representative images of migrating cells through a 0.8 micron trans-well towards the indicated attractants (2% FBS, -Ctl; 50% FBS, +Ctl; or 10% FBS, experimental). Right, mean fold-change ± SEM of invading cells compared to 2% FBS (-Ctl) set as 1.0. (* $p < 0.05$, **** $p < 0.0001$, as determined by one-way ANOVA with Dunnett post-test, comparing all groups to 2% FBS (-Ctl)).

Figure S7 – Pancreas area analysis and classifications

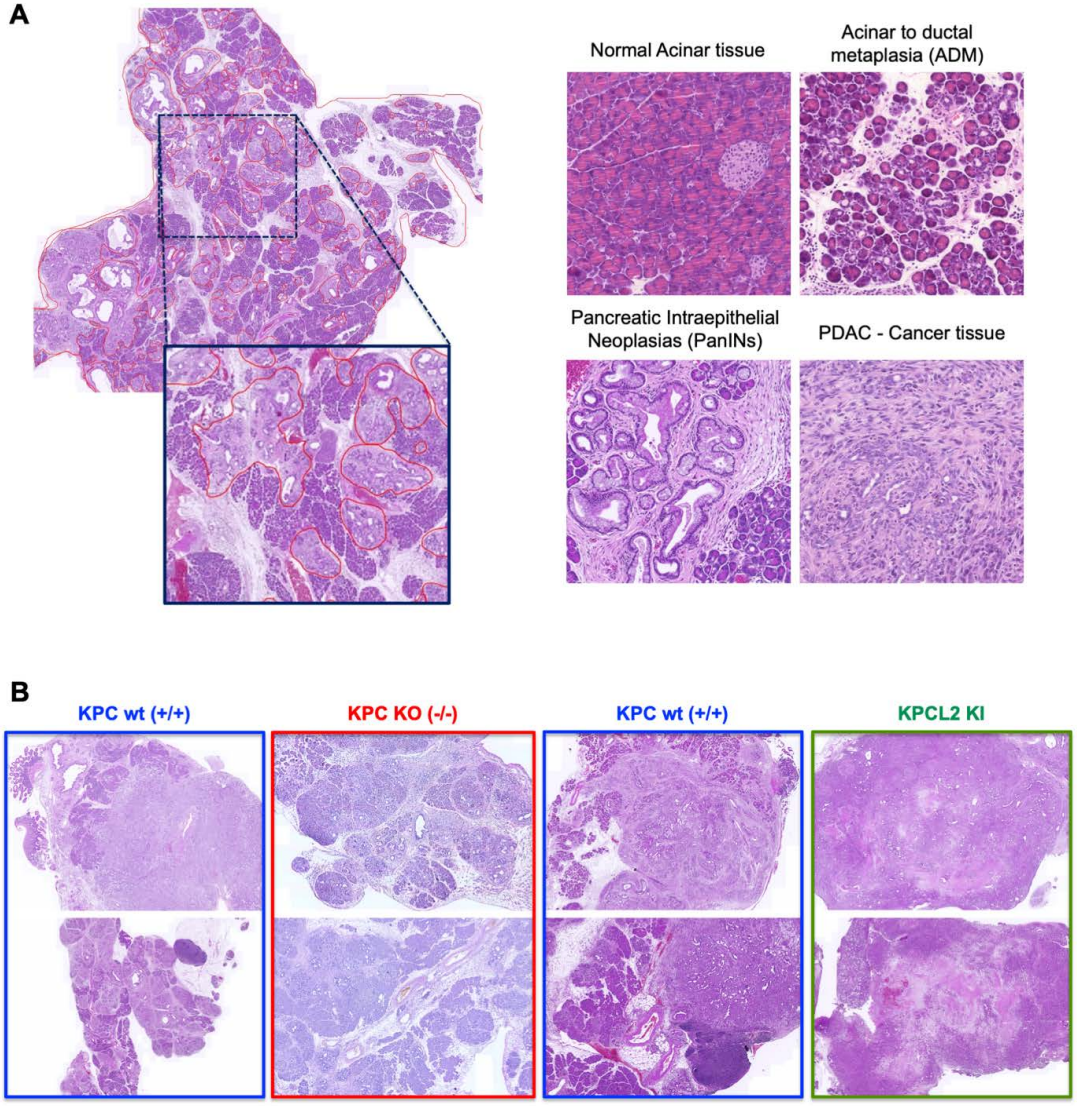

Figure S7: Pancreas area analysis and classifications.
(A) Representative hematoxylin and eosin (HE)-stained section of a KPC tumor. Total area and sub areas were selected and categorized as severely altered tissue (acinar-to-ductal metaplasia (ADM) and inflammation), pancreatic intraepithelial neoplasias (PanINs I–III), cancer tissue (PDAC) or normal acinar tissue.
(B) Representative H&E images of pancreata from indicated genotypes.

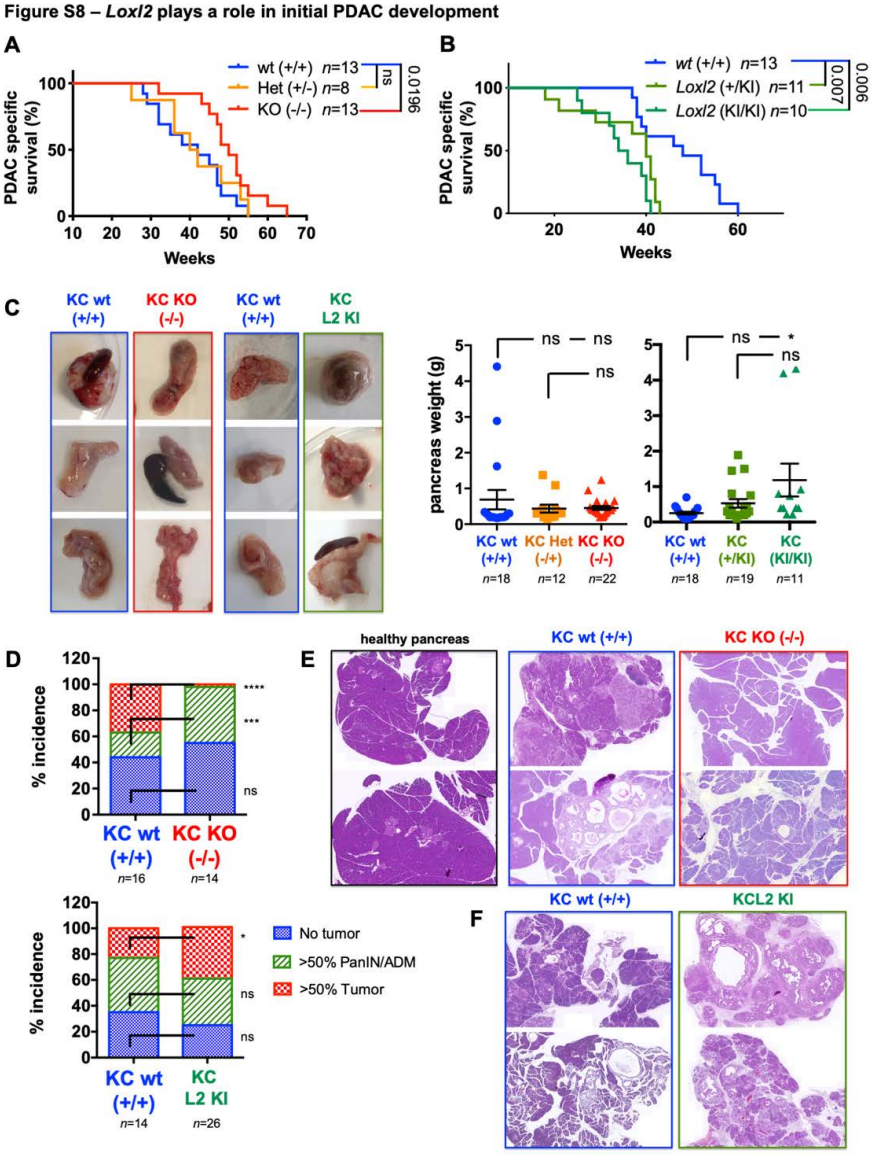

Figure S8: *Loxl2* plays a role in initial PDAC development.

(A) Survival of KC wild-type (+/+), HET KC (KC;*Loxl2*$^{+/-}$), and KO KC (KC;*Loxl2*$^{-/-}$) mice. All mice died of PDAC associated disease at the indicated times (p value is shown, ns = not significant, log-rank (Mantel–Cox) test). Calculated median survivals are: wild-type (+/+): 42; HET KC (KC;*Loxl2*$^{+/-}$): 41; and KO KC (KC;*Loxl2*$^{-/-}$): 50 weeks.

(B) Survival of KC wild-type (+/+), KC;R26L2$^{+/KI}$ and KC;R26L2$^{KI/KI}$ mice. All mice died of PDAC associated disease at the indicated times (p value is shown, log-rank (Mantel–Cox) test). Calculated median survivals are: wild-type (+/+): 48; KC;R26L2$^{+/KI}$: 40; and KC;R26L2$^{KI/KI}$: 35 weeks.

(C) Representative images (left) and mean pancreas weight ± SD (right) in wild-type (+/+), HET KC (KC;*Loxl2*$^{+/-}$), KO KC (KC;*Loxl2*$^{-/-}$), and wild-type (+/+), KC;R26L2$^{+/KI}$ and KC;R26L2$^{KI/KI}$ mice, determined at 37-40 weeks post birth. (* $p < 0.05$, ns = not significant, as determined by one-way ANOVA with Tukey post-test).

(D) Quantification of tissue area in mouse pancreata from wild-type (+/+) KC and HET KC (KC;*Loxl2*$^{+/-}$) mice (blue, n = 16) and KO KC (KC;*Loxl2*$^{-/-}$) mice (red, n = 14) (top) and in wild-type (+/+) KC mice (blue, n = 14) and KCL2^{KI} (KC;R26L2$^{+/KI}$ and KC;R26L2$^{KI/KI}$) mice (green, n = 26) (bottom), determined at 37-40 weeks post birth, categorized as normal acinar tissue (No tumor), cancer tissue (Tumor) or Pancreatic intraepithelial neoplasias (PanINs I–III) / acinar-to-ductal metaplasia (ADM). (* $p < 0.05$, *** $p < 0.001$, **** $p < 0.0001$, ns = not significant, as determined by contingency analysis, two-sided Fisher's exact test).

(E-F) Representative H&E images of healthy pancreata or pancreata of the indicated genotypes.

Figure S9 – Overexpression of *Loxl2* enhances tumor metastasis

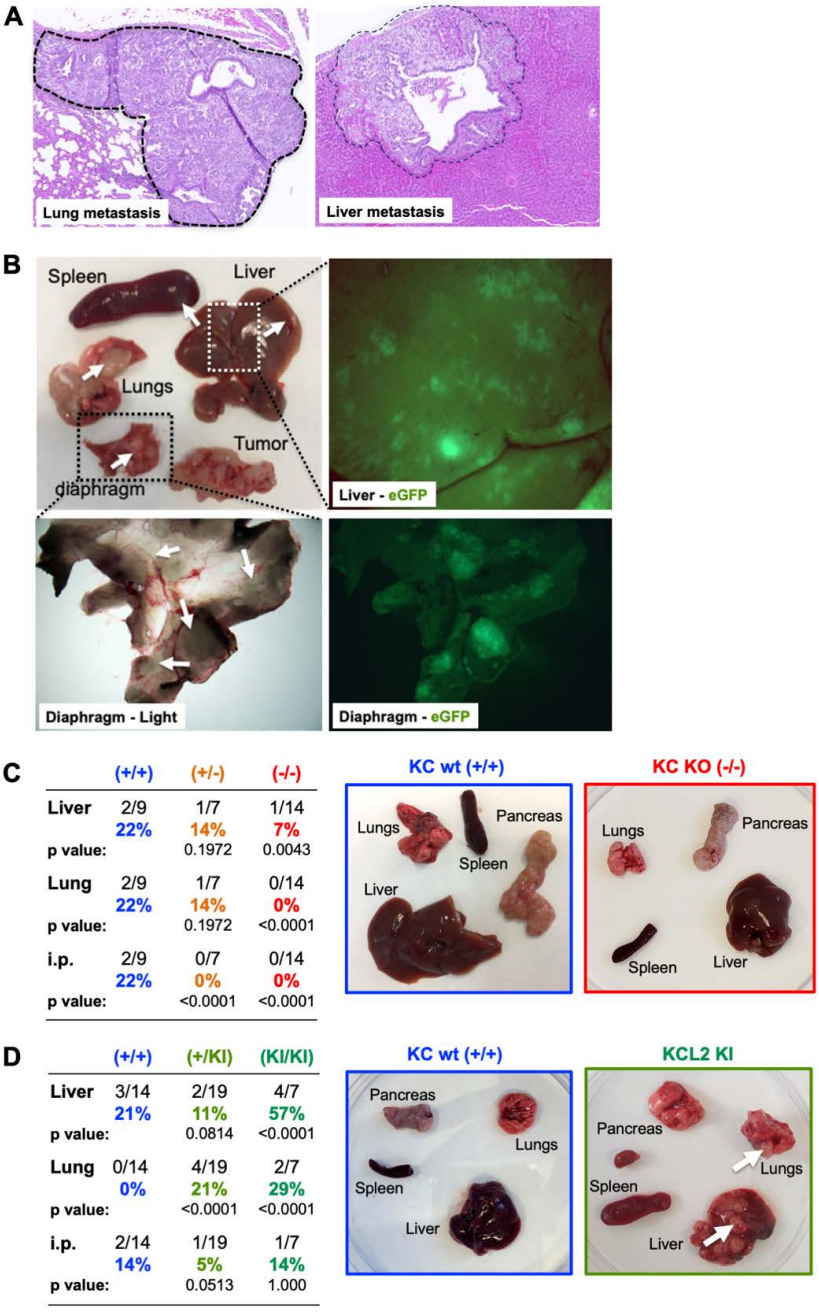

	(+/+)	(+/-)	(-/-)
Liver	2/9	1/7	1/14
	22%	14%	7%
p value:		0.1972	0.0043
Lung	2/9	1/7	0/14
	22%	14%	0%
p value:		0.1972	<0.0001
i.p.	2/9	0/7	0/14
	22%	0%	0%
p value:		<0.0001	<0.0001

	(+/+)	(+/KI)	(KI/KI)
Liver	3/14	2/19	4/7
	21%	11%	57%
p value:		0.0814	<0.0001
Lung	0/14	4/19	2/7
	0%	21%	29%
p value:		<0.0001	<0.0001
i.p.	2/14	1/19	1/7
	14%	5%	14%
p value:		0.0513	1.000

Figure S9: Overexpression of *Loxl2* enhances tumor metastasis

(A) Representative hematoxylin and eosin (HE)-stained section of PDAC metastatic lesions in the lung or liver of a 24-week-old wt KPC mouse.

(B) Representative images of PDAC tumors and metastases from a KPC;R26L2$^{KI/KI}$ mouse. Shown are photographs of explanted organs (white arrows indicate metastases), and light and fluorescent images of liver and diaphragm taken with a fluorescent dissecting microscope.

(C-D) Percent incidence of liver, lung and i.p. metastasis in (C) wild-type (+/+) KC, HET (KC;*Loxl2*$^{+/-}$) and KO (KC;*Loxl2*$^{-/-}$) mice or (D) wild-type (+/+) KC, KC;R26L2$^{+/KI}$ and KC;R26L2$^{KI/KI}$ mice determined at 37-40 weeks post birth. (p values are indicated, as determined by contingency analysis, two-sided Fisher's exact test). (right) Images of explanted organs from mice of the indicated genotypes (white arrows indicate metastases).

Figure S10 – Expression of EMT-associated proteins in tumor samples

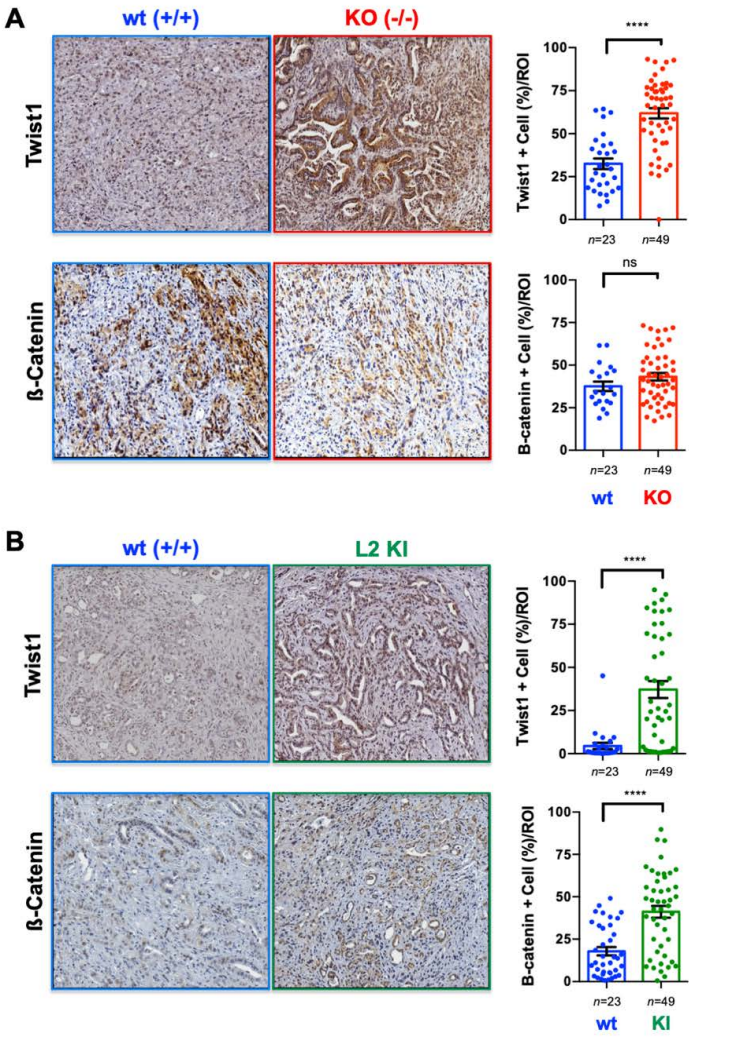

Figure S10: Expression of EMT-associated proteins in tumor samples

(A) Left: Representative immunohistochemical stainings for Twist1 and ß-catenin expression in tumor sections from wild-type (+/+) KPC and KO KPC (KPC;*Loxl2*$^{-/-}$) mice. Scale bar = 250µm. Right: Quantification of percent positive (+) cells/ROI. (**** $p < 0.0001$, ns = not significant, as determined by unpaired Student's t test).

(B) Left: Representative immunohistochemical stainings for Twist1 and ß-catenin expression in tumor sections from wild-type (+/+) KPC and KPCL2^{KI} (KPC;R26L2$^{KI/KI}$) mice. Scale bar = 250µm. Right: Quantification of percent positive (+) cells/ROI. (**** $p < 0.0001$, as determined by unpaired Student's t test).

Figure S11 – Expression of E-cadherin in tumor samples

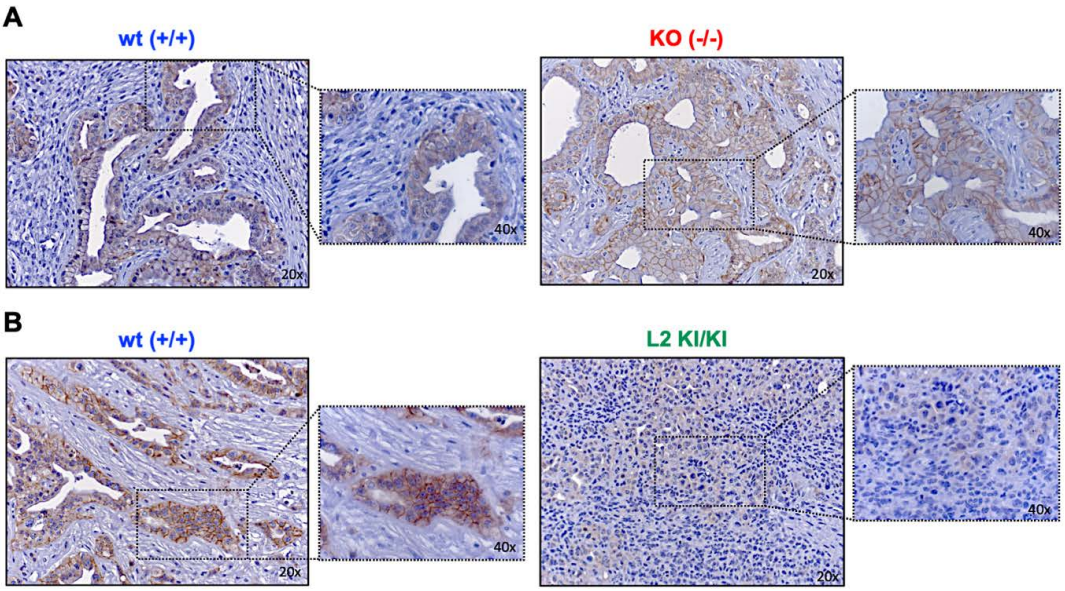

Figure S11: Expression of E-cadherin in tumor samples.
(A-B) Representative immunohistochemical staining of E-cadherin in tumor sections from (A) wild-type (+/+) KPC and KO KPC (KPC;*Loxl2*$^{-/-}$) mice or (B) wild-type (+/+) KPC and KPCL2^{KI} (KPC;R26L2$^{KI/KI}$) mice. 20X magnification. Insets indicate area that is shown on the right at 40X.

Figure S12 – Loxl2 levels do not affect TGFß responsiveness

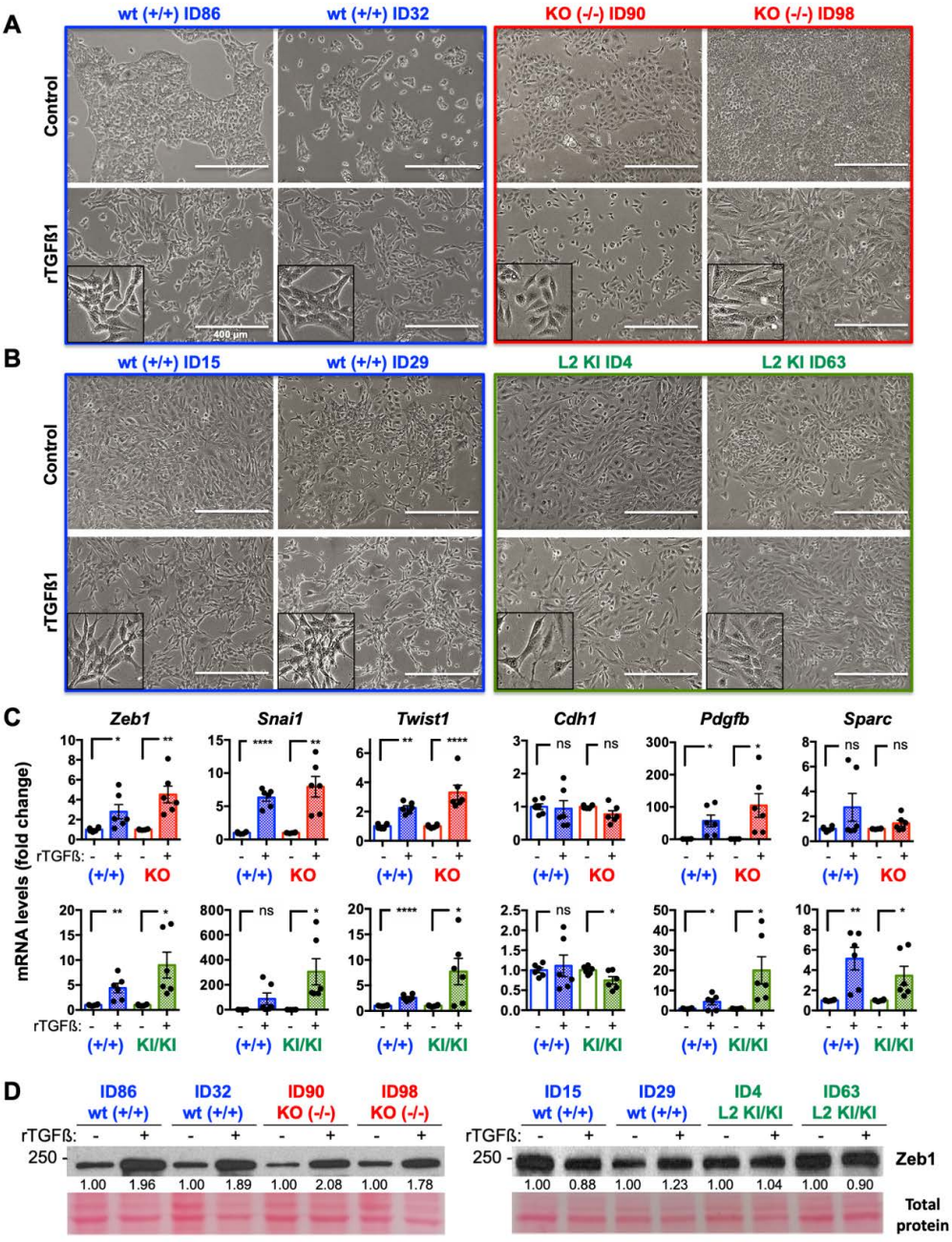

Fig S12: Loxl2 levels do not affect TGFß responsiveness

(A-B) Representative light micrographs of tumor cell lines derived from (A) wild-type (+/+) KPC tumors (ID86 and ID32, blue) and KO KPC (KPC;*Loxl2*$^{-/-}$) tumors (ID90 and ID98, red) or (B) wild-type (+/+) KPC tumors (ID15 and ID29, blue) and KPCL2^{KI} (KPC;R26L2$^{KI/KI}$) tumors (ID4 and ID63, green). Scale bar = 400µm. Inset = 4X amplification.

(C) RT-qPCR analysis of mean fold change ± SEM of indicated EMT- or metastasis-related genes in tumor cell lines derived from the indicated genotypes following treatment with rTGFß1 (5ng/ml) daily for 3 days (* $p < 0.05$, ** $p < 0.01$, **** $p < 0.0001$, ns = not significant, as determined by unpaired Student's t test).

(D) WB analysis of Zeb1 in samples from (A-C). Ponceau S staining served as a normalization control. Zeb1 densitometric values, normalized to total protein, are indicated.

Figure S13 – Loxl2 levels do not affect Osm responsiveness

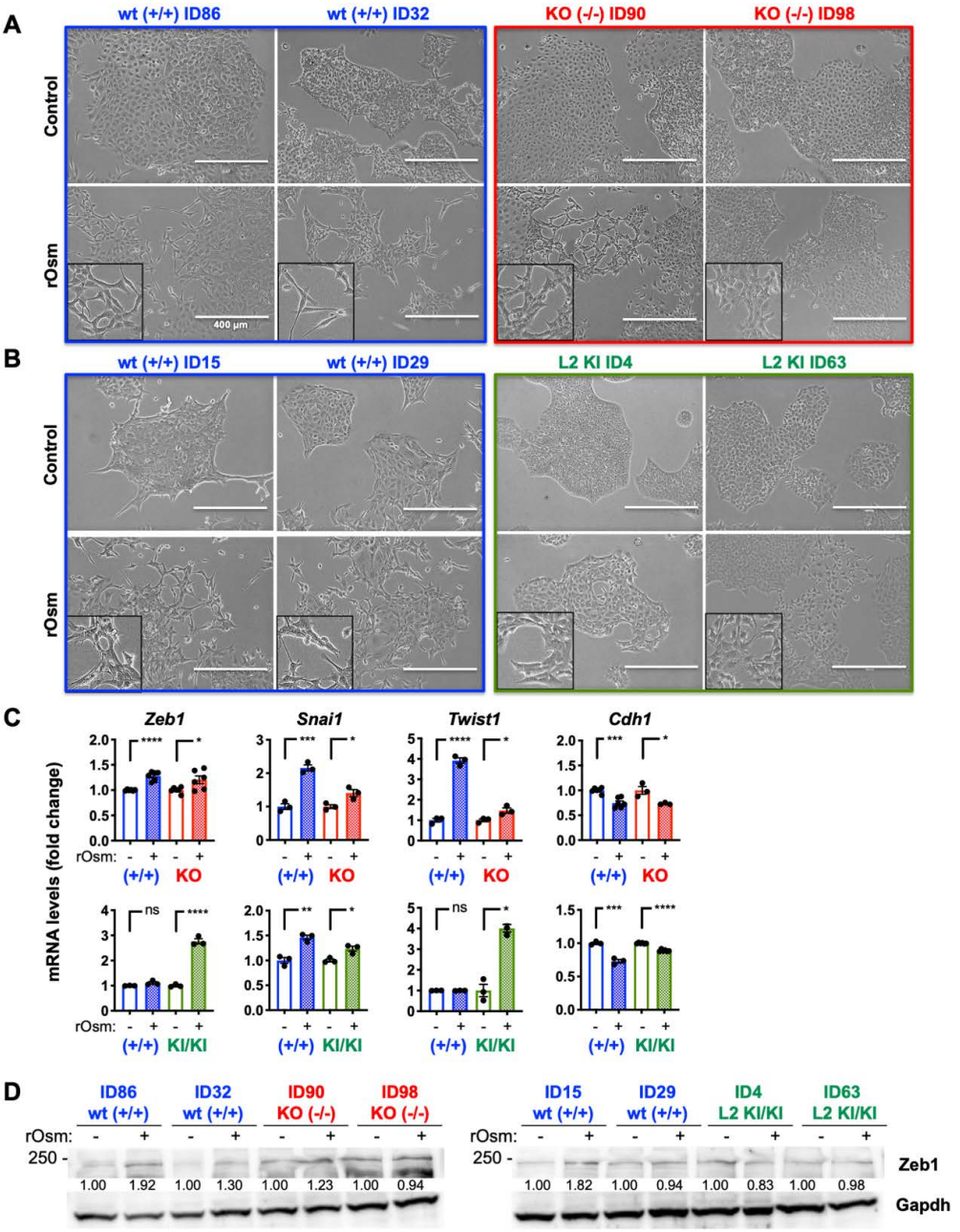

Fig S13: Loxl2 levels do not affect Osm responsiveness

(A-B) Representative light micrographs of tumor cell lines derived from (A) wild-type (+/+) KPC tumors (ID86 and ID32, blue) and KO KPC (KPC;*Loxl2*$^{-/-}$) tumors (ID90 and ID98, red) or (B) wild-type (+/+) KPC tumors (ID15 and ID29, blue) and KPCL2^{KI} (KPC;R26L2$^{KI/KI}$) tumors (ID4 and ID63, green). Scale bar = 400µm. Inset = 4X amplification.
(C) RT-qPCR analysis of mean fold change ± SEM of indicated EMT-related genes in tumor cell lines derived from the indicated genotypes following treatment with rOsm (200ng/ml) daily for 3 days (* $p < 0.05$, ** $p < 0.01$, *** $p < 0.001$, **** $p < 0.0001$, ns = not significant, as determined by unpaired Student's t test).
(D) WB analysis of Zeb1 in samples from (A-C). Gapdh served as a normalization control. Zeb1 densitometric values, normalized to Gapdh values, are indicated.

Figure S14 – Loxl2 and tumor formation

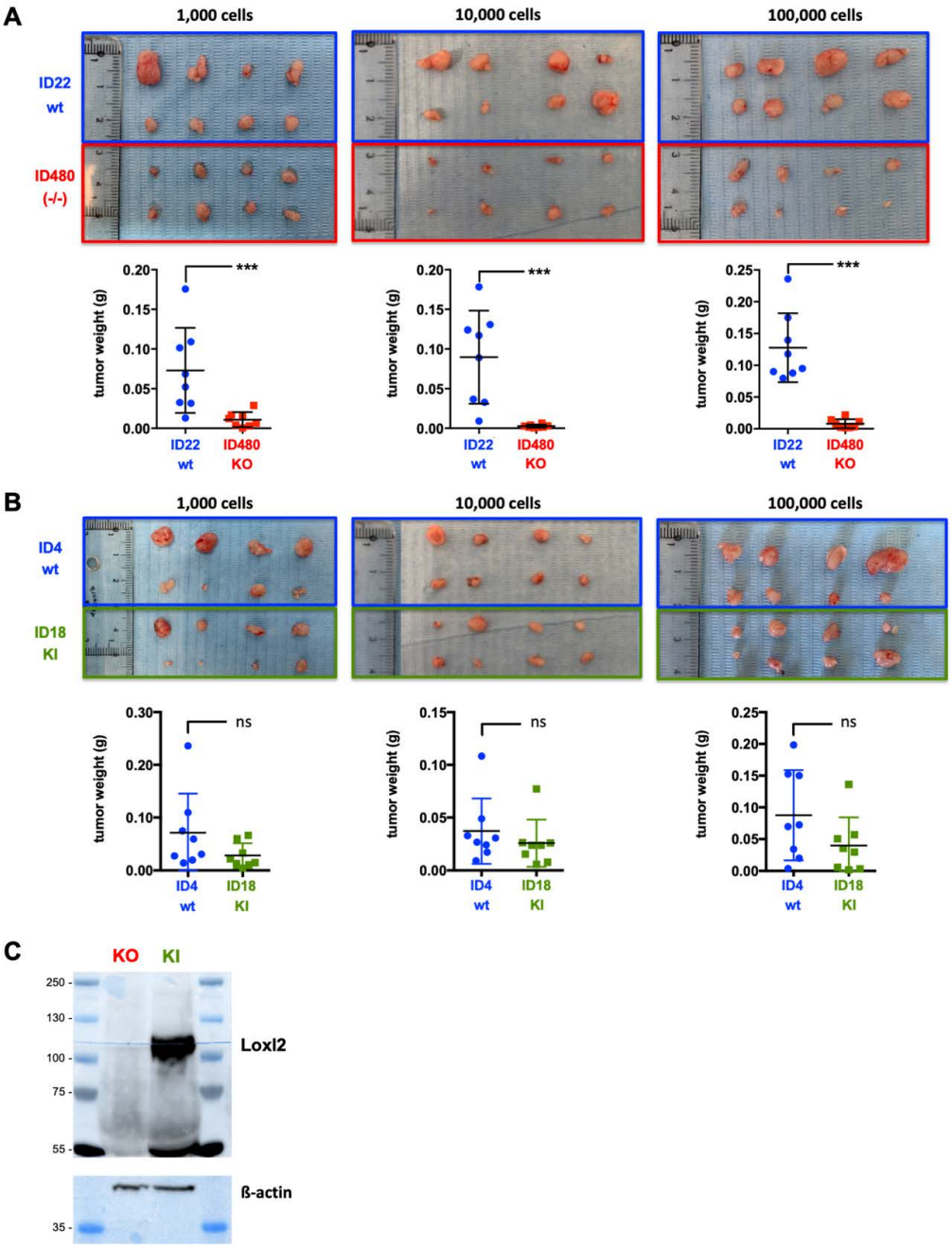

Figure S14: Loxl2 and tumor formation.

(A) Images of tumors formed (top) and mean tumor weight ± SD (bottom) for wild-type (+/+) KPC cells (ID22, blue) and KO KPC (KPC;*Loxl2*$^{-/-}$) cells (ID80, red), determined at 14 weeks post injection in immunocompromised nude mice at the indicated dilutions.

(B) Images of tumors formed (top) and mean tumor weight ± SD (bottom) for wild-type (+/+) KPC cells (ID4, blue) and KPCL2^{KI} (KPC;R26L2$^{KI/KI}$) cells (ID18, green), determined at 14 weeks post injection in immunocompromised nude mice at the indicated dilutions.

(C) Western blot analysis of Loxl2 in concentrated cell supernatants from KPCL2^{KO} and KPCL2^{KI} cells cultured for 48h in the absence of serum. ß-actin served as a loading control. The membrane was cut.

Figure S15 – Expression of mechanosignaling-associated proteins in tumor samples

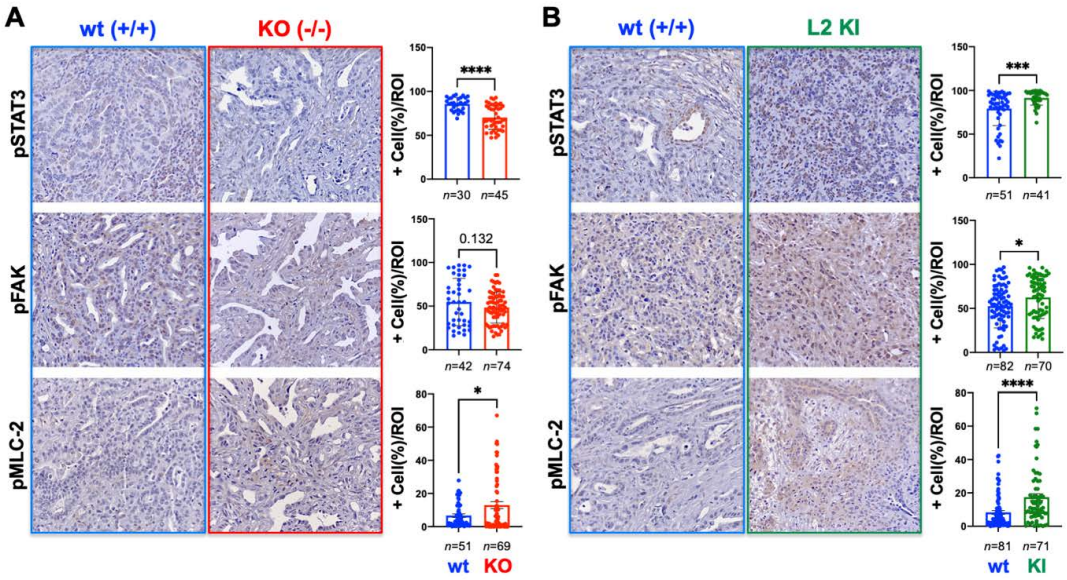

Figure S15: Expression of mechanosignaling-associated proteins in tumor samples.
(A) Left: Representative immunohistochemical stainings of pSTAT3, pFAK, pMLC-2 expression in tumor sections from wild-type (+/+) KPC and KO KPC (KPC;*Loxl2*$^{-/-}$) mice. Right: Quantification of percent positive (+) cells/ROI. (* $p < 0.05$, **** $p < 0.0001$, as determined by unpaired Student's t test).
(B) Left: Representative immunohistochemical stainings of pSTAT3, pFAK, pMLC-2 expression in tumor sections from wild-type (+/+) KPC and KPCL2^{KI} (KPC;R26L2$^{KI/KI}$) mice. Right: Quantification of percent positive (+) cells/ROI. (* $p < 0.05$, *** $p < 0.001$, **** $p < 0.0001$, as determined by unpaired Student's t test).

Figure S16 – Immune cell profile in tumors with different levels of Loxl2

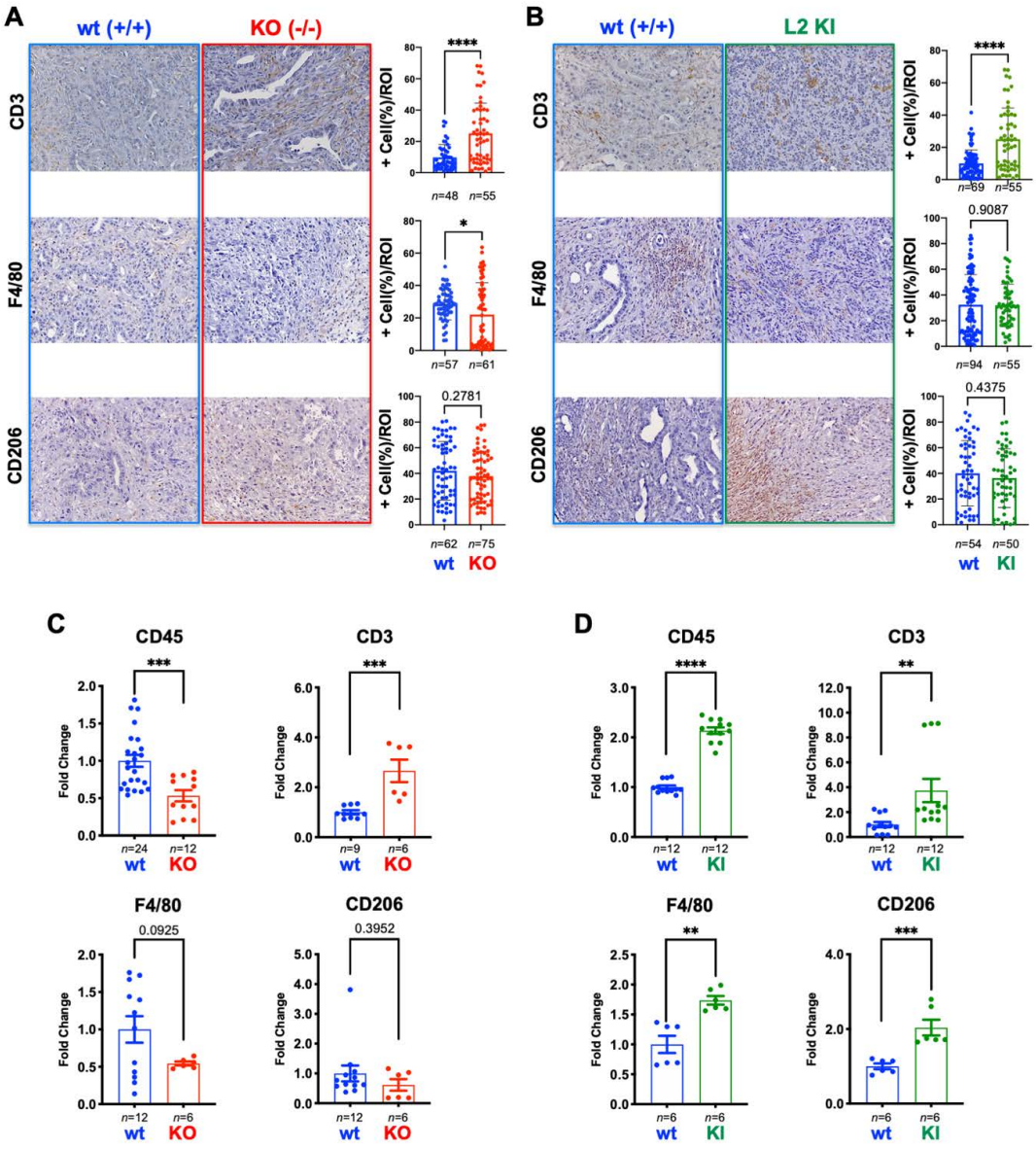

Figure S16: Immune cell profile in tumors with different levels of Loxl2.

(A) Left: Representative immunohistochemical stainings of CD3, F4/80 and CD206 expression in tumor sections from wild-type (+/+) KPC and KO KPC (KPC;*Loxl2*$^{-/-}$) mice. Scale bar = 250µm. Right: Quantification of percent positive (+) cells/ROI. (* $p < 0.05$, **** $p < 0.0001$, as determined by unpaired Student's t test).

(B) Left: Representative immunohistochemical stainings of CD3, F4/80 and CD206 expression in tumor sections from wild-type (+/+) KPC and KPCL2^{KI} (KPC;R26L2$^{KI/KI}$) mice. Scale bar = 250µm. Right: Quantification of percent positive (+) cells/ROI. (**** $p < 0.0001$, as determined by unpaired Student's t test).

(C-D) Mean fold-change ± SD of the percentage of CD45+, CD3+, F4/80+ or CD206+ cells in freshly digested PDAC tumors from 18-week old (C) wild-type (+/+) KPC or KO KPC (KPC;*Loxl2*$^{-/-}$) mice, or (D) wild-type (+/+) KPC or KPCL2^{KI} (KPC;R26L2$^{KI/KI}$) mice. (** $p < 0.01$, *** $p < 0.001$, **** $p < 0.0001$, as determined by unpaired Student's t test).

SUPPLEMENTARY VIDEOS

Supplementary Video 1: Movement and cell scattering of Panc354 cells in cultured with control medium

Supplementary Video 2: Movement and cell scattering of Panc354 cells in cultured with macrophage-conditioned medium